

UNCLASSIFIED

AD 264226

*Reproduced
by the*

ARMED SERVICES TECHNICAL INFORMATION AGENCY
ARLINGTON HALL STATION
ARLINGTON 12, VIRGINIA



UNCLASSIFIED

NOTICE: When government or other drawings, specifications or other data are used for any purpose other than in connection with a definitely related government procurement operation, the U. S. Government thereby incurs no responsibility, nor any obligation whatsoever; and the fact that the Government may have formulated, furnished, or in any way supplied the said drawings, specifications, or other data is not to be regarded by implication or otherwise as in any manner licensing the holder or any other person or corporation, or conveying any rights or permission to manufacture, use or sell any patented invention that may in any way be related thereto.

264228

U. S. A R M Y
TRANSPORTATION RESEARCH COMMAND
FORT EUSTIS, VIRGINIA

TCREC TECHNICAL REPORT 61-37

VTOL DOWNWASH IMPINGEMENT STUDY

SUMMARY REPORT

Task 9R38-01-017-29

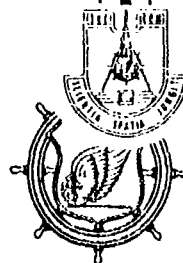
Contract DA 44-177-TC-655

August 1961

NCX
61-4-60

prepared by :

HILLER AIRCRAFT CORP
Palo Alto, California



HEADQUARTERS
U. S. ARMY TRANSPORTATION RESEARCH COMMAND
Fort Eustis, Virginia

FOREWORD

This report summarizes the results of research performed by Hiller Aircraft Corp. under Army Contracts DA 44-177-TC-500 and DA 44-177-TC-655. The test data are presented in TREC Technical Reports 60-58, 60-67, and 61-34. This work represents a part of a research program, still in progress, which is devoted to the determination of the flow patterns and characteristics of the downwash induced by helicopters and VTOL vehicles as well as to the evaluation of the resultant effects of the downwash on the aircraft, supporting equipment, personnel, and landing area.

A narrated 16-millimeter motion picture film has been prepared, showing some of the tests conducted and results observed during the test program, and can be obtained on a loan basis by addressing requests to:

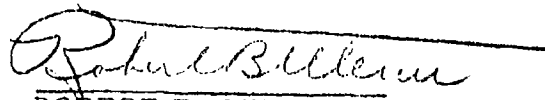
Commanding Officer
U. S. Army Transportation Research Command
Fort Eustis, Virginia.

The report has been reviewed by this Command and is considered to be technically sound. The report is published for the exchange of information and the stimulation of ideas.

FOR THE COMMANDER:

APPROVED BY:


ROBERT R. GRAHAM
USATRECOM Project Engineer


ROBERT B. MERCER
Captain, TC
Asst Adjutant

Task Number 9R38-01-017-29
Contract DA 44-177-TC-655
August 1961

VTOL DOWNWASH IMPINGEMENT STUDY
SUMMARY REPORT

Hiller Engineering Report No. 61-3

Prepared by:
Hiller Aircraft Corp.
Palo Alto, California

for
U. S. ARMY TRANSPORTATION RESEARCH COMMAND
FORT EUSTIS, VIRGINIA

Prepared by:

A. Morse - Aerodynamicist

Project Engineer:

H. Newhouse

Approved by:

R. Anderson - Chief Project Engineer
R. Carlson - Chief, Aero-Structures
S. Sherby - Vice President, Engineering and Research

TRECOM Personnel:

R. Graham - Project Engineer

TABLE OF CONTENTS

	Page
FORWARD	i
LIST OF FIGURES	v
LIST OF SYMBOLS	vii
1. SUMMARY	1
2. CONCLUSIONS	2
3. RECOMMENDATIONS	4
4. INTRODUCTION	5
5. DISCUSSION	6
6. EVALUATION	22
7. REFERENCES	58
APPENDIX: Calculations Leading to a Solution of the Field Maximum Dynamic Pressure in Ground Effect.	59
DISTRIBUTION	73

LIST OF FIGURES

<u>Figure</u>		<u>Page</u>
1	Test Site, Velocity Survey Test Equipment	24
2	Typical Dynamic Pressure Profile	25
3	Variation of $(q/q_m)_{max.}$ with x/R	26
4	Field Maximum $(q/q_m)_{F.M.}$ Parallel to Ground	27
5	Field Maximum Dynamic Pressure Ratio	28
6	Interaction Between Jet Wake and Surface Wind	29
7	General Arrangement, Test Equipment, Side by Side Flow Adapter	30
8	Dynamic or Total Pressure Decay	31
9	Total Pressure Profiles (Side by Side Ducts)	32
10	General Arrangement, Test Equipment, Plenum Chamber	33
11	General Arrangement, Test Equipment, Annular Nozzle Flow Adapter	34
12	Profile of Eroded Sand	35
13	Impingement Pattern, Side by Side Flow Adapter	36
14	Flow Rate Profiles (Side by Side Ducts)	37
15	Erosion Rate Produced by a Single One Foot Diameter Duct	38
16a	Flow Rate Profiles)	39
16b	Flow Rate Profiles) 2-Foot Ducted Propeller and	40
17a	Flow Rate Profiles) Side by Side Ducts	41
17b	Flow Rate Profiles)	42
18a	Flow Rate Profiles)	43
18b	Flow Rate Profiles) of 2-Foot Duct	44
19a	Flow Rate Profiles)	45
19b	Flow Rate Profiles - Side by Side Ducts	46
20	Flow Rate Profiles - 2-Foot Duct	47
21	Flow Rate Profiles with Variable Z/D	48
22	Flow Rate Profiles Comparing Soils IV A and IV B	49
23	Particle Size Distribution	50
24	Relative Diameter of Eroded Section Soil Condition I B	51
25	Relative Diameter of Eroded Section Soil Condition III A	52
26	Relative Diameter of Eroded Section Soil Condition IV A	53

Figure

		<u>Page</u>
27	Pressure, Depth Correlation of Water Tests	54
28	Comparison of Dynamic Pressure Profiles After Impingement	55
29	Variation of Maximum Dynamic-Pressure Ratio with Radial Location	56
30	Observed Spray Height	57

LIST OF SYMBOLS

a	= wave amplitude	feet
A_L	= duct exit flow area	square feet
C	= constant	none
D	= jet diameter	feet
D_P	= propeller diameter	feet
D_H	= diameter of eroded area	feet
f	= wave frequency	c.p.s.
h	= height measured from the undisturbed impingement surface	feet
K	= constant	appropriate
m	= mass flow rate	slugs per second
P	= local pressure	pounds per square foot
P_0	= ambient pressure	pounds per square foot
P_t	= total pressure	pounds per square foot
q	= local dynamic pressure	pounds per square foot
q_m	= mean dynamic pressure in the free jet at the source	pounds per square foot
q_{max}	= maximum surface dynamic pressure at survey location under consideration	pounds per square foot

q_{FM}	= the maximum dynamic pressure in the flow field produced by a jet or rotor	pounds per square foot
q_{CR}	= surface dynamic pressure required to initiate erosion	pounds per square foot
R	= radius	feet
T	= thrust	pounds
VL	= volume loading $\left(\frac{\text{particle volume}}{\text{max. projected area}} \right)$	inches
w	= disk loading (T/A)	pounds per square foot
x	= radial distance measured along the surface from the impingement point	feet
y	= distance measured along the impingement surface from the geometric center of non-circular configurations	feet
Z	= vertical height of the developed free jet above the surface	feet
θ	= thrust axis inclination	degrees
ϕ	= azimuth measured in the surface plane in a clockwise direction from the propeller axis projection, from a direction along the plowed furrows, or from the major axis of a configuration	degrees

Nomenclature Used for Soil Condition

- I Lean Clay (CL)
 - A. Bladed Section
 - B. Flowed Section (Flat)
 - C. Flowed Section (Furrowed)
 - D. Grassy Area (Unmowed)
 - E. Grassy Area (Freshly Mowed)

II Fat Clay (CH)
A. Weathered
B. Bladed

III Sand (SP)
A. Dry
B. Wet

IV Sandy Gravel (GW)
A. As Deposited
B. Sprinkled and Compacted

V Water
A. Fresh

This system of soil condition nomenclature was used to provide a complete cross reference between this report and References 2 and 3. A single designation was used which consists of:

- 1) A Roman numeral that designates the type of soil.
- 2) An alphabetical symbol that designates the soil preparation.
- 3) The test number assigned at the time the test was conducted.

A designation can consist of the first two parts when reference is made to a series of tests.

Example: Data designated I B 25.

This data refers to test number 25, which was conducted over a plowed flat surface of lean clay.

1. SUMMARY

This report summarizes the results of previous tests, which included disk loadings from 2 to 150 pounds per square foot and Z/D ratios from .25 to 3. During these testing velocity surveys over non-eroding surfaces, erosion rates for various soils, and deflections in water surfaces were obtained. The configurations used in the tests were: open propellers, ducted propeller, side by side jets, and Ground Effect Machines (GEM) of the plenum and annular nozzle type.

When considering a circular jet impinging normal to a smooth surface under no wind conditions, and for radial distances greater than two and one-half times the jet radius, the following conclusions can be made: The velocity parallel to the surface depends upon the total thrust and not upon the disk loading. The field maximum surface velocity is a function of disk loading and Z/D. The radial surface jet thickness increases linearly with the distance from the impingement point.

Although the surface dynamic pressure, at large radial distances, is proportional to the total thrust, it is the field maximum dynamic pressure that initiates the erosion. The onset of erosion is therefore determined by the disk loading, Z/D, and the critical dynamic pressure for the particular surface.

Light surface winds will deflect the radial jet above the surface and transport small particles back to the impingement area. This constitutes considerable operational difficulty.

With the exception of gravel most natural surfaces erode at surface dynamic pressures below 3 or above 150 pounds per square foot. Relatively free surface material, i.e., sand, dust, water, etcetera, erode when the surface dynamic pressure is 3 or less. Packed sod, concrete, macadam, vegetation, etcetera, will all withstand surface dynamic pressures in excess of 150 pounds per square foot. Obviously loose surface dust, water, etcetera, will be blown free.

Gravel is normally composed of a large range in particle sizes, for example the gravel used in these tests had particle sizes from .05 millimeters to 40 millimeters. Low disk loadings move the very light particles. This erosion may decrease with time. At disk loadings of 60 to 100 pounds per square foot the erosion rate was rapid and the largest particles were blown free of the eroding area.

Saturating sand with water decreased the erosion rate considerably; at a disk loading of 125 pounds per square foot the activity consisted of a continuous process of drying and then eroding of the surface.

2. CONCLUSIONS

If a homogenous surface is assumed the two parameters, the surface critical dynamic pressure and field maximum dynamic pressure (q_{FM}), determine if erosion will be encountered. The field maximum dynamic pressure varies directly with disk loading and inversely but in a non-linear fashion with Z/D .

When a circular jet is formed as a result of producing lift, the maximum surface dynamic pressure, at radial distances greater than $x/R = 2.5$, is dependent upon the total thrust. The thickness, or height, of the radial flow depends upon the distance from the impact point; i.e., the zero velocity line is given by $h = Cx$ where $.250 \approx C \approx .268$.

Deviations in the surface from the smooth flat surface used in the velocity survey tests do not have a large effect on the field maximum dynamic pressure, or the onset of erosion.

Additional velocity survey data is required to evaluate the influence of surface winds or forward velocity, changes in jet geometry, and contoured surfaces designed to minimize the surface area that must be protected to prevent erosion.

Each surface will have at least one critical dynamic pressure where the onset of erosion takes place. A large percentage of the natural surfaces will have two or more critical dynamic pressures: The first in the order of 1 to 3 pounds per square foot where the loose surface material begins to move; and the second, usually a much higher value, where the top soil breaks free and begins to move. When a thick surface layer is composed of free particles in the range of .1 millimeter or smaller, a severe dust problem is encountered. These small particles do not readily settle back to the surface once disturbed.

Relatively hard dust-free surfaces, such as macadam or concrete, may have large free particles on the surface. These particles are completely exposed to the surface flow and will move at low dynamic pressures. The danger here is primarily to personnel or other aircraft, as these particles travel away from the impingement area.

Jet impingement on water produces spray at surface dynamic pressures above 2 to 3 pounds per square foot and the spray height increases with disk loading.

A surface wind or forward velocity has a strong influence on the flow field, such that lightweight eroded particles are lifted out of the downwash flow field on the upwind side and returned toward the jet.

When landing sites can be selected, areas with light vegetation or damp areas should be used. Surface traffic should be avoided as much as possible. Prepared landing areas should be kept clean, particularly if used by more than one aircraft.

3. RECOMMENDATIONS

The problems associated with the downwash impingement are complex and, as with most problems, there does not appear to be an ideal solution. The best solution will probably result in a compromise, which depends to some extent on the assumed mission. To make intelligent compromises the problem must be well defined and the effect of all variables known.

To date there are no known test results that clearly define the influence of surface winds (or forward velocity). Small scale tests would prove to be most advantageous as the work could be conducted indoors where controlled, simulated winds could be provided for the tests. Selected geometric jet shapes should be used as a systematic variable in scale tests to determine the characteristics of non-circular jet flow fields. Although most lifting devices tend to produce circular jets, there is a possibility of using secondary, non-circular jets (which may possess more desirable characteristics, such as lower decay rates) to effectively control the basic flow.

It has been shown in this report that, at a constant disk loading, the field maximum dynamic pressure increases with decreasing Z/D . When designing an aircraft with the capability of operating at low Z/D ratios to reduce power requirements, or provide greater overload capability, consideration should be given to the increase in the field maximum dynamic pressure and the intended operational environment of the aircraft.

For future VTOL aircraft, surface erosion and associated impingement problems should be considered in the preliminary design of the aircraft. Special filtration or other protective equipment for the aircraft and/or for the landing area may be necessary to meet specific operational requirements.

4. INTRODUCTION

The operation of helicopters and vertical lift types of aircraft from unprepared surfaces presents problems associated with the downwash or slipstream impingement. Among these problems are the effects on: the pilot; the aircraft physically and operationally; tactical operation of the aircraft; and danger to ground personnel and equipment resulting from dust and debris set in motion by the downwash or slipstream.

Hiller Aircraft Corp. was awarded Contract DA 44-177-TC-500 in 1958 to study the characteristics of the downwash from VTOL aircraft. Tests were conducted with propellers and a ducted fan. The results of this test program were presented in Reference 1.

In April 1960 Contract DA 44-177-TC-655 was awarded Hiller Aircraft Corp. to conduct additional tests and evaluation of the effects of the downwash impingement on a variety of soil conditions. This test program was conducted at the Corps of Engineers Waterways Experiment Station at Vicksburg, Mississippi. Test sites, soil analysis and general support of the test program were provided by the Waterways Experiment Station. The results of tests with the two-foot diameter ducted fan were presented in Reference 2. Additional tests were conducted with a diffuser and adapters installed on the ducted fan. Side by side flow for VTOL aircraft, an annular nozzle ground effect machine, and a plenum chamber type ground effect machine were simulated. The results of this test program were presented in Reference 3.

The results of these test programs have been analyzed. This analysis, including correlation between the downwash studies and the movement of soil particles, recommendations relative to VTOL aircraft design, and suggestions for future research are presented in this report.

5. DISCUSSION

Mobility of the test equipment was provided through the use of a U. S. Army Model M-54, 5-ton, 6x6 cargo truck with a front-mounted winch (Figure 1). The power was supplied to the propeller by a Ford Model 332 industrial V-8 engine, driving through a five-speed gear box and a right angle drive. The height of the propulsion unit was varied by raising or lowering the boom assembly with the winch cable. Due to the flexibility of the boom assembly and cable, accurate settings of Z/D were difficult. When the thrust was applied the load in the cable and boom was relieved and the Z/D would change from the static position. For the adapter tests (Reference 3) where small changes in height resulted in large variations of Z/D, a support strut and screw jack were used to provide close control over the adapter height.

The Z/D was established before the propulsion unit was engaged; therefore, when surface erosion was incurred the Z/D changed as the erosion progressed. In some tests the eroded section had a maximum depth of 14 inches, which produces a significant change in Z/D. With the exception of the water tests, all Z/D ratios are pre-operation values.

5.1 VELOCITY SURVEY

5.1.1 GENERAL FLOW FIELD

The velocity survey tests were conducted to provide some insight into the basic flow field. Complicating factors were eliminated where possible. Tests were conducted during minimum wind over flat, non-eroding surfaces. In effect the problems associated with the impingement, such as dust, flying particles, etcetera, were eliminated so as to reveal the basic flow in its simplest form. The test equipment, test procedures, and the data obtained are presented in Reference 1. The concern here is not with the tests but what has been accomplished as a result of the velocity survey tests.

An over-all examination of the impingement will be necessary before the velocity survey test results can be discussed in detail. The jet, which is a result of producing lift at zero or low forward speeds, does not dissipate readily. When this jet strikes the surface, the velocity normal to the surface is reduced to zero, and the energy is converted to pressure that accelerates the flow away from the impingement area. After the maximum velocity is reached, the surface flow continues away from the high pressure region, where diffusion and viscous forces eventually reduce the velocity to an insignificant value. The flow field was observed through the use of the tuft boards, and quantitative data were obtained from pitot pressure measurements. A general view of the test arrangement and the equipment used is shown in Figure 1.

The initial jet mean dynamic pressure (q_m) provides a convenient basis for reducing much of the data to non-dimensional form for a jet that issues from a nozzle (as a ducted propeller or turbojet engine) the following relation exists:

$$q_m = \frac{T}{2 A_L} = \frac{W}{2}$$

For an open propeller or rotor where the flow contracts downstream of the reference area, the mean dynamic pressure is related to disk loading by:

$$q_m = W.$$

The diameter used for the analysis of open propellers or rotors is the contracted slipstream diameter:

$$D = .707 D_p.$$

The results of the velocity surveys are presented in terms of the dynamic pressure ratios (q/q_m) , $(q/q_m)_{\max}$, and $(q/q_m)_{FM}$. The term (q/q_m) represents the ratio between the dynamic pressure (q) and mean jet dynamic pressure (q_m). The term $(q/q_m)_{\max}$ represents the maximum surface dynamic pressure obtained at some specific x/R location, referred to the mean jet dynamic pressure. The term $(q/q_m)_{FM}$ is reserved to describe the maximum surface dynamic pressure irrespective of the location in the flow field, again referred to the initial mean jet dynamic pressure.

5.1.2 DYNAMIC PRESSURE VARIATIONS IN THE FLOW FIELD

The dynamic pressure data obtained from the tests were plotted for fixed conditions of Z/D and x/R to obtain the dynamic pressure variation with height above the surface. This dynamic pressure profile, shown in Figure 2, is typical of all obtained. The maximum value (q/q_m) was obtained at several radial stations and a cross plot of $(q/q_m)_{\max}$ versus x/R was made for each value of Z/D tested. Figure 3 shows the change in maximum dynamic pressure with radial location that results from the impingement of a circular jet normal to a flat surface.

The flow follows the sequence shown below:

First, the exit flow velocity decreases, converting dynamic pressure to static pressure.

Second, the flow accelerates along the surface until the static pressure is reduced to ambient and the surface dynamic pressure is a maximum.

Third, the velocity decreases with increasing radial distance due to a combination of diffusion and viscous forces.

The velocity decay obtained from a circular jet is such that it fits the curve:

$$(q/q_m)_{\max} = \pi \rho \left(\frac{K}{x/R} \right)^2, \quad \text{where } K = 26.8 \text{ was determined in Reference 4 and shown to give good correlation with full scale tests.}$$

This equation can be used to show that the surface dynamic pressure at a given radial location is a function of total thrust and not disk loading:

If a ducted propeller is assumed:

$$q_m = w/2 = \frac{T}{2A} = \frac{T}{2\pi R^2}$$

$$q_{max.} = \pi \left(\frac{K}{x/R}\right)^2 \frac{T}{2\pi R^2} = \frac{T}{2} \left(\frac{K}{x}\right)^2$$

or for a non-ducted propeller where

$$q_m = w = \frac{T}{\pi R^2}$$

$$q_{max.} = T \left(\frac{K}{x}\right)^2$$

The boundary between the jet surface flow and ambient still air is a function of the radial distance from the impact point. The equation of the zero velocity line is given in Reference 1 as $h/D = K x/R$ where $.125 \leq K \leq .134$. If both sides of the equation are multiplied by $2R$ the following equation is obtained:

$$h = Cx \text{ where } .25 \geq C \geq .268.$$

The above solutions are valid when $x > 2R$. To find the field maximum dynamic pressure, the disk loading and Z/D must be known.

Because the maximum dynamic pressure from each pressure profile was used to plot Figure 3, the maximum dynamic pressure (for a given Z/D) from Figure 3 is the maximum value in the flow field and is therefore called the field maximum dynamic pressure. The curve of $(q/q_m)_{FM}$ (Figure 4) is of prime importance as the onset of erosion is governed by the soil classification parameters and the field maximum dynamic pressure. If the soil critical dynamic pressure (q_{CR}) is known, the disk loading and Z/D combination required to start erosion can be found, i.e.

$$q_{F.M.} = (q/q_m)_{F.M.} \times q_m$$

for a ducted propeller $q_m = w/2$

$$\therefore q_{F.M.} = (q/q_m)_{F.M.} w/2$$

or

$$w = \frac{2 q_{F.M.}}{(q/q_m)_{F.M.}}$$

where $(q/q_m)_{F.M.}$ is a function of Z/D as shown in Figure 4 and $q_{F.M.} = q_{CR}$ when erosion starts.

If $q_{F.M.}$ is less than q_{CR} , there will be no erosion at the point of maximum dynamic pressure and therefore no erosion will take place at any x/R location. If $q_{F.M.}$ is greater than q_{CR} , erosion will start and continue to take place until the local maximum dynamic pressure $[(q/q_m)_{max.} \text{ at } x/R]$ decreases below that required to propagate the erosion. An indication of the relative severity of the erosion problem can be obtained by the excess in the field maximum dynamic pressure above that required (q_{CR}) to initiate erosion.

Figure 3 is useful in determining the approximate extent of the particle cloud. When the local maximum dynamic pressure $[(q/q_m)_{max.} \text{ at } x/R]$ decreases below that required to sustain the particles, they will settle back to the surface. One must be very cautious when using Figure 3 for this purpose, as surface winds or excessive erosion can greatly influence the flow pattern.

As was stated previously, the surface dynamic pressure has a maximum value in the vicinity of one diameter from the centerline of rotation; beyond this distance the surface dynamic pressure is a function of the total thrust and not the disk loading. It cannot be emphasized too strongly that it is the field maximum dynamic pressure that determines whether or not a surface will be eroded and the field maximum dynamic pressure is a function of disk loading and proximity to the ground.

The analysis in the appendix provides a solution for the field maximum dynamic pressure as influenced by the normal parameters of disk loading, power loading, and geometry. The most direct method of reducing the field maximum dynamic pressure (see Equation 10 appendix) is to reduce the disk loading; however, this parameter is usually determined by other requirements. Figure 2 of the appendix indicates that significant reductions in the field maximum dynamic pressure (q_6 of the appendix) can be obtained by small changes in Z/D if the design Z/D is ≤ 0.5 ; if the design Z/D is ≥ 1.0 the reduction in the maximum surface dynamic pressure obtainable by increasing Z/D are insignificant.

Figure 4 of the appendix indicates that, when the equivalent Z/D ratio is less than one, significant reductions in the field maximum dynamic pressure (for constant disk loading) are made possible by using jets of high aspect ratio.

5.1.3 EFFECTS OF TILTING THE THRUST VECTOR

Velocity survey tests were conducted at $\theta = 0^\circ$, 30° , and 60° thrust axis inclination, the results of which are presented in Reference 1. The surveys at $\theta = 30^\circ$ and $\theta = 60^\circ$ did not include as many x/R stations, where velocity profiles were obtained, as did the $\theta = 0^\circ$ tests. Because of the rapid change of $(q/q_m)_{\max}$ with x/R and the relatively few profiles available, the validity of the $(q/q_m)_{\text{FM}}$ versus Z/D (Figure 5) curves for $\theta = 30^\circ$ and $\theta = 60^\circ$ is questionable. The values given by the curves were obtained from tests; however, it is possible that higher values existed at points where no measurements were made.

If the jet decay curve is compared with the $(q/q_m)_{\text{FM}}$ curve for zero thrust inclination (Figure 4) one finds that the maximum surface dynamic pressure is approximately equal to the stream dynamic pressure from the jet decay curve, provided the points of comparison are at the same Z/D value. These two curves represent the two extremes in thrust axis inclination (0° and 90°). If the flow can strike the surface and turn through 90 degrees with little or no loss in total pressure, then it should turn through a lesser angle with no greater loss in total pressure. One would conclude that, as Z/D has been defined in this report, the curves of Figure 5 should differ by the cosine of the tilt angle. The data indicate greater losses for $\theta = 30^\circ$ and $\theta = 60^\circ$. Assuming the data to be correct, large angles (and therefore significant losses in vertical thrust) are required to appreciably reduce the field maximum dynamic pressure.

5.1.4 EFFECT OF SURFACE WINDS

The general radial flow pattern after impingement without surface wind is near the surface. The surface velocity increases with radial distance from impingement, until the static pressure is equal to ambient pressure, and then it decreases beyond this point (Figure 3). When a surface wind (or forward velocity) is imposed upon the flow pattern, the shearing forces between the wind and radial flow on the upwind side produce a surface flow profile similar to that shown in Figure 6. This shearing action causes the radial flow to separate from the surface when the surface dynamic pressure is slightly greater than the free stream dynamic pressure. After separation the radial velocity component decreases and the free stream and jet flow mix and blow back toward the source.

If a jet is impinging on a smooth erodible surface, and the disk loading is sufficiently high, particles will be entrained and carried

radially outward in the decreasing velocity flow. If there is no surface wind a point will be reached where there is insufficient velocity to sustain the particle and it will fall to the surface and come to rest. It is of little consequence whether the particle momentum at low radial distances is sufficient to carry it beyond the area where the velocity will no longer keep it in motion. Thus the particle would not be returned toward the source regardless of its physical characteristics. On the other hand, if there is a surface wind (or forward motion) the particle may or may not (depending upon its physical characteristics) return to the immediate surface. Very light particles will be trapped in the rolling up flow, lifted higher above the surface and returned toward the jet. This action has been observed and recorded on motion picture film.

If the surface wind velocity is of the same relative magnitude as the field maximum surface dynamic pressure, the jet flow and the entrained particles will be swept back, leaving the upwind side of the jet clear. The dust cloud will form downwind of the impingement point.

As long as the surface remains relatively flat there should exist a definite relationship between the field maximum dynamic pressure, the jet diameter, the wind velocity and the height of the dust cloud. At constant altitude increasing disk loading will move the mixing region upwind and increase the height of the dust cloud in relation to the increase in the maximum surface dynamic pressure; increasing wind velocity will shift the dust cloud downwind. Increasing altitude will decrease the cloud in relation to the dynamic pressure decay curve.

5.1.5 EFFECT OF GEOMETRY AND MULTIPLE SOURCE

The two-foot diameter ducted propeller used in References 1 and 2 was fitted with a diffuser. Two adapters, for mounting on the diffuser exit, were constructed. One adapter provided a pair of jets, each one foot in diameter and two feet between centers, and the other adapter simulated an annular nozzle ground effect machine (GEM). The annular nozzle GEM had a total area (base plate plus nozzle) of 5.2 square feet, with a .6-inch thick jet inclined toward the base at 45 degrees. The open end of the diffuser was used to simulate a plenum chamber GEM. The detailed test data have been presented in Reference 3.

The three configurations discussed above were operated over a flat non-eroding surface at fixed heights while gage pressure measurements of the flow field were made.

5.1.5.1 SIDE BY SIDE DUCTS (FIGURE 7)

The gage (total minus ambient) pressures for the side by side ducts were measured at a disk loading of 44.6 pounds per square foot and at an exit height of 1.56 feet ($Z/D = 1.56$). Seven gage pressure profiles were obtained at x/R ratios between one and three, with the total pressure rake located at $\theta = 0^\circ$, 45° , and 90° (see Figure 8). These profiles show a maximum gage pressure in the region of $x/R = 1.33$ to 1.67. It must be remembered that these profiles are gage pressure and not dynamic pressure profiles. The difference is the use of total pressure minus ambient rather than total minus static pressure. The static pressure was determined (for the two-foot duct) to decrease rapidly to ambient pressure at $x/R = 2$. High gage pressures at $x/R < 2$ are, therefore, not indicative of high velocities; beyond $x/R = 2$ the gage and dynamic pressure are identical. A comparison of the radial dynamic pressure decay rates obtained from the side by side ducts and the single, two-foot duct are shown by Figure 8. It is interesting to note that the minor axis of the side by side ducts system (where considerable concentrations of dust were observed) apparently does not experience higher maximum velocities than the other areas; it does, however, indicate a lower decay rate and thus higher velocities at radial stations beyond $x/R = 2.5$. Comparing the profiles (Figure 9) it can be seen that the minor axis flow is much greater at high values of h/D ($h/D = 1$), apparently due to the fact that the maximum pressure is above the surface at the centerline of the system. The fact that the maximum velocities along the major and minor axes are approximately equal is to be expected. The stream reaches stagnation pressure at the impingement point, and when two jets are used one would expect three stagnation points, the third being midway between the two jet stagnation points. A vertical component of flow along the minor axis might be expected due to the secondary impingement of the ground flows along this axis.

5.1.5.2 PLENUM CHAMBER (FIGURE 10)

The plenum chamber was operated at three disk loadings, 4.36, 9.40, and 31.25 pounds per square foot ($A_L = 5.955$ square feet), at a constant height of three inches. The plenum chamber can be considered as a non-circular jet operated in very close proximity to the ground plane. The data obtained indicates a field maximum dynamic pressure ratio of approximately 1.7. To compare this to the curve of Figure 4 an equivalent diameter must be used. The comparison used here will be equivalent $(Z/D)_e$ based on the value of $(A_L/Z)_e$, where for a circular jet $(A_L/Z)_e = \frac{1}{4Z/D}$; therefore, $(Z/D)_e = \frac{1}{4(A_L/Z)_e}$

The value obtained by making the indicated substitution is $(Z/D)_e = .0994$. This point $[(Z/D)_e = .0994, q/q_m = 1.7]$ is in close agreement with Figure 4. If an equivalent diameter based only on the exit area is used, the $(Z/D)_e$ value would be essentially the same in this case $[(Z/D)_e = .0908]$.

5.1.5.3 ANNULAR NOZZLE (FIGURE 11)

The annular nozzle was operated at three disk loadings, 2.31, 9.64 and 16.6 pounds per square foot (based on total area $A_u + A_b = 5.2$ square feet). The data obtained from these tests cannot be compared directly with Figure 4, due to the difference in geometry, except to note that the maximum value of $P_t/w/2 = 2.75$ is considerably above the range of Figure 4.

5.2 SURFACE EROSION

5.2.1 INTRODUCTION

The results of the surface erosion tests have been presented in Reference 2 (two-foot diameter duct tests) and in Reference 3 (adapter tests).

Tests were conducted over various surfaces with different preparations. Wave rods were used during the tests over water, providing a continuous record of the water elevation at each of the rods. Particle traps were located in the flow field where possible, providing information on the quantity of material trapped at the various geometric locations. From this information the weight flow (pounds per minute) of material passing through a square foot area normal to the surface was obtained and designated as the flow rate. Plots of h/D versus flow rate were constructed for each test where this information was available. For the two-foot duct tests over gravel, the size of the largest particle in each trap was recorded and plots of h/D versus volume loading constructed. The volume loading (V.L.) was obtained by dividing the particle volume by the maximum projected area, thus reflecting not only the size but also the particle shape. Measurements were made of the eroded section, and 16 millimeter motion picture coverage of the majority of tests was obtained. The Waterways Experiment Station supported the testing by furnishing the test sites and performing necessary soil tests for classification of the soils and for determination of the condition of the soils at the time of tests. The results are included in References 2 and 3.

All recorded information was presented regardless of its apparent value because the nature of the erosion and the controlling parameters were not clearly defined. This data represents the time average during the test duration, normally about one minute, during which the flow pattern, in many cases, was observed to change completely. It is the general trends and order of magnitude that are to be considered in the sections dealing with surface erosion.

5.2.2 FLOW RATE PROFILES

To determine if the side by side ducts were influenced by the diffuser and to determine the area of mutual interference, three duct

configurations of the side by side ducts were operated over dry sand at a disk loading of 60 pounds per square foot and at a Z/D of 1.5. The first configuration was with standard eight-inch nozzles. The nozzles were extended to 26 $\frac{1}{2}$ inches in the second configuration and in the third configuration one of the standard eight-inch nozzles was diverted by a 12 by 28 by 46 inch box (see Reference 3). Observations made during the tests indicated that the flow changed from radial to vertical 50 seconds after the tests started. The eroded sections were very similar (profiles are shown in Figure 12) except near the center of the single duct test where a damp area was noted. The conclusion was drawn that the diffuser was not influencing the impingement, and the region of mutual interference was limited to the narrow wedge area shown in Figure 13. By comparing the flow rate profiles (Figure 14) it can be concluded that the results of tests III A 33 and III A 41 were very similar. The flow rate profiles of test III A 46 show considerably less erosion than the first two tests. The difference in the $y/R = 6$ curve "A" is to be expected as this trap was located on the minor axis of the system and one duct was diverted during this test. The total erosion of one duct was calculated by integration of the profiles shown in Figure 12 to determine the eroded volume. The total erosion thus calculated was plotted on Figure 15 and shows essentially the same relationship between the three tests as did the flow rate profiles.

5.2.3 COMPARISON OF CONFIGURATION BY FLOW RATE PROFILES

The sand tests were used to determine the similarity between the flow rate curves for the two-foot diameter duct and the side by side one-foot diameter ducts due to the relative uniformity of the sand. With the duct exit close to the surface ($Z/D = .5$) reasonable agreement is obtained (Figures 16a and 16b). The agreement is somewhat better at low values of x/R where the surface wind is not such a powerful influencing factor. The test results at $Z/D = 3$ show the correlation to be essentially independent of Z/D (Figures 17a and 17b); again greater deviations in flow rate appear at the highest values of x/R . Generally better correlation is found near the ground surface. This would be in the higher velocity area where the surface wind would have less influence. A small difference in moisture content and density existed between the tests. At the time the two-foot diameter duct was tested, the dry density of the sand was 92.2 pounds per cubic foot and the moisture content was between .5 and 1.3 percent. The side by side ducts were tested when the dry density of the sand was between 90.5 and 91.5 and the moisture content was between .2 and .4 percent.

It appears that the flow rate values obtained with the two-foot duct and the side by side ducts can be compared directly with no loss in generality.

5.2.4 DISCUSSION OF TRENDS AND RELATIONSHIPS

One of the most predominant trends that appeared in the results of tests over the various soil conditions was the increase in flow rate with increasing disk loading. This is to be expected as the surface dynamic pressure varies directly with disk loading. The flow rate profiles Figures 16 and 17 cannot be made independent of disk loading in a manner similar to that used for the dynamic pressure profiles (see Figure 2) because the slope of the flow rate vs. h/D curve changes with disk loading. The high flow rates at large h/D values and high disk loading (seen in Figures 16 and 17) are most probably due to the vertical projection of material resulting from the erosion.

The effect of increasing Z/D is shown in Figures 18a and 18b. There is a greater decrease in flow rate between $Z/D = .5$ and $Z/D = 1.5$ than between $Z/D = 1.5$ and $Z/D = 3$. This would be expected from the velocity profile results, namely the field maximum dynamic pressure curve (Figure 4).

The relative erodibility of the different soils is compared in Figures 19a and 19b. The flow rate parameter is apparently affected by time. Therefore w , Z/D and time have been held constant in Figure 19. The erosion rate of the "as deposited" river gravel (IV A) is high, and large flow rates are found at large values of h/D where these particles could inflict heavy damage if they are large in size. It will be shown in section 5.2.4.1 that the particles actually were of considerable size.

The flow rates obtained from dry sand (III A), flat plowed lean clay (I B), and the plowed and furrowed lean clay (I C), show that considerable quantities of material were in motion. A lower density material will have a greater volume flow at the same flow rate. These small particles are largely responsible for: the erosion of rotor or propeller blades, contamination of lubricants, and are the primary source of visibility problems.

Figure 20 shows the effect of disk loading and X/R on the flow rate profiles for the "as deposited" river gravel, and Figure 21 shows the effect of Z/D . The effect of moisture and compaction was to reduce the erosion (Figure 22).

5.2.4.1 VOLUME LOADING

The relative size of the particles can be obtained from the volume loading curves. Volume loading is the particle volume divided by its maximum cross sectional area; therefore, the diameter (in inches) of

a spherical particle would be equal to $3/2$ the volume loading. For a rectangular particle the V.L. would equal the smallest dimension. The particle sizes and the capture location can be obtained from Figure 23. In addition to the particle size these curves shed some additional light on the nature of the flow pattern after erosion has taken place. The "sprinkled and compacted" gravel curves show larger particles near the surface and smaller particles at high h/D values. The flow rate curves show the "as deposited" gravel had greater flow rates, and the slope of the "as deposited" gravel curves is greater than those for the "damp, compacted" gravel. From this it can be concluded that as the erosion takes place the high velocity flow lifts above the surface. When operating over the "as deposited" gravel the higher erosion rate creates a hole in a shorter period of time. The flow lifts above the surface, carrying with it the larger particles. The "damp, compacted" gravel had a lower total erosion rate, thus the hole took longer to form and the flow remained along the surface. This resulted in a higher flow rate near the surface and a lower flow rate at higher h/D 's than with the "as deposited" gravel.

5.2.5 MEASUREMENTS OF ERODED AREA

After completing a test, the size of the eroded area was measured to determine the diameter and depth of the resulting impression. In Reference 2 the relative depression diameter was plotted against disk loading with flagged symbols to denote the time variable, as the diameter of the eroded section would be expected to increase with time. Figure 24 is a reproduction of the $Z/D = 3$ and $Z/D = .5$ data from Reference 2, wherein the standard test time was three minutes. Data from Reference 3 is also included, wherein the test time was one minute. The diameter of the depression directly beneath one of the ducts was used for D_H of the side by side ducts to facilitate comparison. It should be noted that reasonably good correlation exists in spite of the marked difference in test time. In this case the depression depth was small compared to the diameter, viz. for the two-foot duct at 125 pounds per square foot, the depression was approximately eight feet in diameter and only eight inches at the deepest point. The flat plate model would provide a fair simulation of this condition, and the rapid decrease in dynamic pressure with x/R would reduce the velocity below the critical value for this soil at a given x/R regardless of test time.

The existence of two D_H/D ratios for the two-foot duct tests over dry sand at a constant disk loading may be noted in Figure 25. The larger circle had a distinct boundary where the sand first settled back to

the surface, within this circle was an undisturbed region, and the eroded section was at the center. As the disk loading decreases the two curves approach the same value and therefore must close when the loading is just sufficient to start erosion. The data from the side by side ducts and the two-foot duct again show reasonable correlation.

The river gravel eroded slightly at 15 pounds per square foot, and the erosion rate increased with disk loading. At a disk loading of 145 pounds per square foot the two-foot duct produced a total erosion rate of 150 pounds of material per second. During this test a hole 8.5 feet in diameter and 14 inches deep developed in 40 seconds. The depth was limited by a hard surface. Sand settled to the surface to a radial distance (x) of 32 feet, and particles equivalent to $\frac{1}{4}$ inch diameter were found to x = 39 feet. Again the correlation in eroded section diameter (Figure 26) is much better than would be expected. It is seen from Figures 24 to 26 that the actual eroded section is normally between three and five jet diameters even though the surface materials cover a large range in particle size and classification.

5.2.6 WATER TESTS

The water pressure (P_s) in the deepest area of the depression would be the product of the density and depth ($P_s = 62.4 h$). The effective Z/D changes considerably for the side by side duct configuration as the water level changes. This was particularly true for low Z/D tests; therefore, the Z/D was based on the bottom of the depression. A maximum surface dynamic pressure was obtained from the field maximum dynamic pressure curve (Figure 4). In the water tests this high velocity in the depression would not be expected, but the field maximum dynamic pressure would give a good representation of the maximum surface gage pressure, $\therefore P_t - P_o = w/2 (q/q_{in})_{FM}$. The ratio of $P_s/(P_t - P_o)$ as obtained from the test data is shown plotted versus disk loading (Figure 27). At low values of disk loading some of the data obtained with the two-foot duct appears to be very poor, but it must be remembered that the water depressions at the low disk loadings were in the order of $\frac{1}{2}$ inch, while allowance was made for water depressions of two feet. In addition the wave rods were supported above the water surface and the supports interfered with the air flow and hence with the measurements. The one-foot-long rods used on the side by side ducts were supported beneath the surface and only the end of the rod protruded. Thus, better data was obtained, as evidenced by the better correlation.

5.2.6.1 WAVE AMPLITUDE AND FREQUENCY

The wave amplitude increased with disk loading such that at $w = 140$ to 150 pounds per square foot the amplitude was $1/4$ to $1/5$ of a foot. The wave frequency is almost independent of disk loading with an order of magnitude of 2 to 4 cps throughout the disk loading range tested. This data is plotted in References 2 and 3.

5.2.7 ONSET OF EROSION

Although the exact disk loading and Z/D required to initiate erosion was not obtained, a general order of magnitude of the surface dynamic pressure required to start appreciable movement can be determined from the test results. Fine particles of loose, dry material require a surface dynamic pressure of one or two pounds per square foot. Large dust clouds are formed by these particles when their size is .01 to .03 millimeters in diameter. The larger particles such as sand (.2 to .4 millimeters) tend to settle back to the surface unless the wind is strong enough to support them. From the dynamic pressure required to start the erosion of sand (approximately two pounds per square foot) the wind velocity required to sustain these particles might be assumed to be in the neighborhood of 30 and 40 mph.

Water spray was formed when the surface dynamic pressure was three pounds per square foot. The spray at this loading was very close to the surface. The wave frequency was two to four cycles per second with an amplitude of more than $\frac{1}{2}$ inch.

5.2.7.1 VEGETATION

Hard soil surfaces with vegetation showed no erosion of the basic soils at the maximum disk loadings tested (140 pounds per square foot). These surfaces all have fine loose particles on the surface that start in motion when the surface dynamic pressure is 1 to 3 pounds per square foot. These light particles form light dust clouds and the pieces of dried grass or vegetation can mat up on air inlet screens to present a real problem.

5.2.7.2 SAND

The dry sand will begin to move when the surface dynamic pressure is 2 to 3 pounds per square foot. Saturating the sand with water greatly reduces the erosion rate; however, a continuous drying takes place at the surface and some motion would be expected.

5.2.7.3 RIVER GRAVEL

River gravel is always accompanied by some sand. Light sand particles were blown from the surface when the surface dynamic pressure was two to three pounds per square foot. The size of the particles and the height above the surface at which a given particle size was found (Figure 23) increased as disk loading was increased. At ducted propeller disk loadings of 140 pounds per square foot, particles approximately $\frac{1}{2}$ inch in diameter were found at the highest trap location 1.08 duct diameters above the surface. Adding moisture and compacting the surface reduced the flow rates at the higher trap compartments, but did not decrease the flow rate of particle size near the surface. At low disk loadings, 8 to 60 pounds per square foot, the size of the particles trapped near the surface increased. The addition of water apparently washed the fine particles down and exposed a greater number of large particles.

6. EVALUATION

The velocity survey tests have proven to be of considerable importance in providing a general understanding of the erosion problem. The excellent agreement obtained between the velocity survey tests of the two-foot duct and those obtained from a four-inch nozzle (Figures 28 and 29) show that velocity survey work can be conducted with scale equipment that allows accurately controlled conditions.

The critical surface dynamic pressure for dust, dry sand, and water was shown in Reference 5 to be independent of scale effects in the range of duct diameters of one to sixteen inches. The critical dynamic pressures obtained from the two-foot duct tests of Reference 2 are compatible with those of Reference 5. The height at which water spray was observed (Reference 5) was non-dimensionalized and plotted versus the "maximum surface dynamic pressure" (the field maximum dynamic pressure). Two curves were obtained, one for the four-inch nozzle and one for the 16-inch ducted fan. The existence of the two curves was attributed to the small size of the water pan in comparison to the 16-inch ducted fan, and therefore the four-inch nozzle data was considered more realistic. The results of the water tests described in References 2 and 3 are in good agreement with the 16-inch ducted fan tests (Figure 30). The pond used during tests of the two-foot duct and the side by side ducts was approximately 40 feet by 100 feet and 22 inches deep. The size of this pond is considered more than adequate, and the curves obtained from the 16-inch ducted fan and the two-foot ducted propeller are considered representative of full scale. A discrepancy exists with data obtained from full scale turbojet experience (described in Reference 5). This data was in better agreement with the data for the four-inch nozzle.

The velocity survey and soil erosion tests conducted under this program will continue to provide valuable information as the understanding of the problem is extended. As of the present time the data has been examined to determine trends, but in many cases the proper variables required to non-dimensionalize and analyze this data are not available.

A large number of variables have been investigated (Z/D , w , soil conditions and geometry). There is a considerable number that have not been considered. One of the most important of these, surface wind or forward velocity, has been avoided. The tests conducted indicate that the surface wind has a profound influence upon the

problem, and light winds are normal in practical operation. The geometry was varied to some extent; however, the analysis of Appendix I indicates appreciable changes in the field maximum dynamic pressure are brought about through variations in geometry. The basic assumptions upon which the analysis depends are subject to criticism; however, reasonable agreement has been obtained with the data from the plenum chamber, annular nozzle, and the ducted configurations used in these tests.

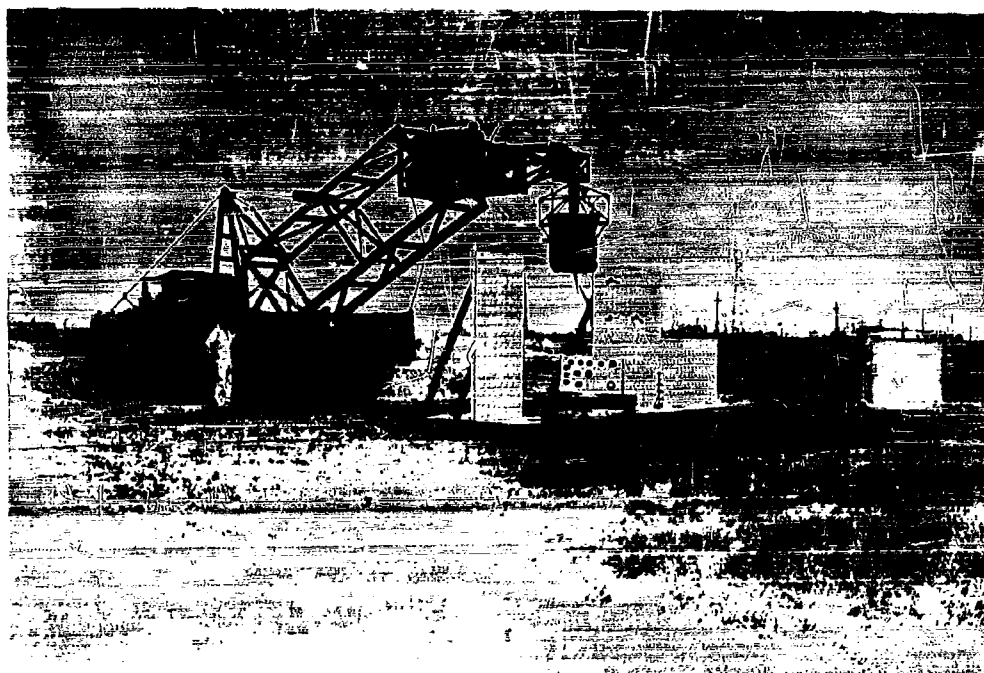


FIG. 1. TEST SITE, VELOCITY SURVEY TEST EQUIPMENT

2-FOOT DUCTED PROPELLER

$Z/D = 1.0$ $x/R = 3.0$

$\theta = 0$ Degrees

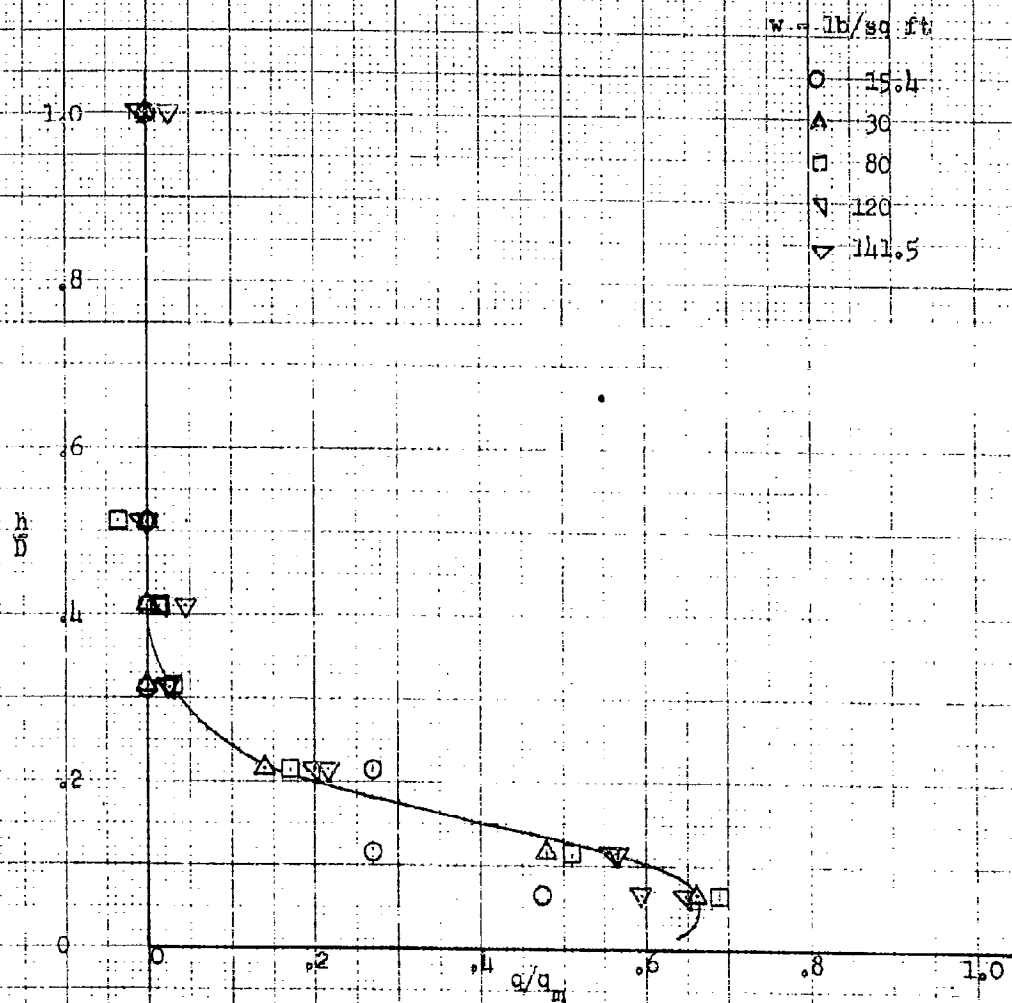


FIGURE 2 TYPICAL DYNAMIC PRESSURE PROFILE

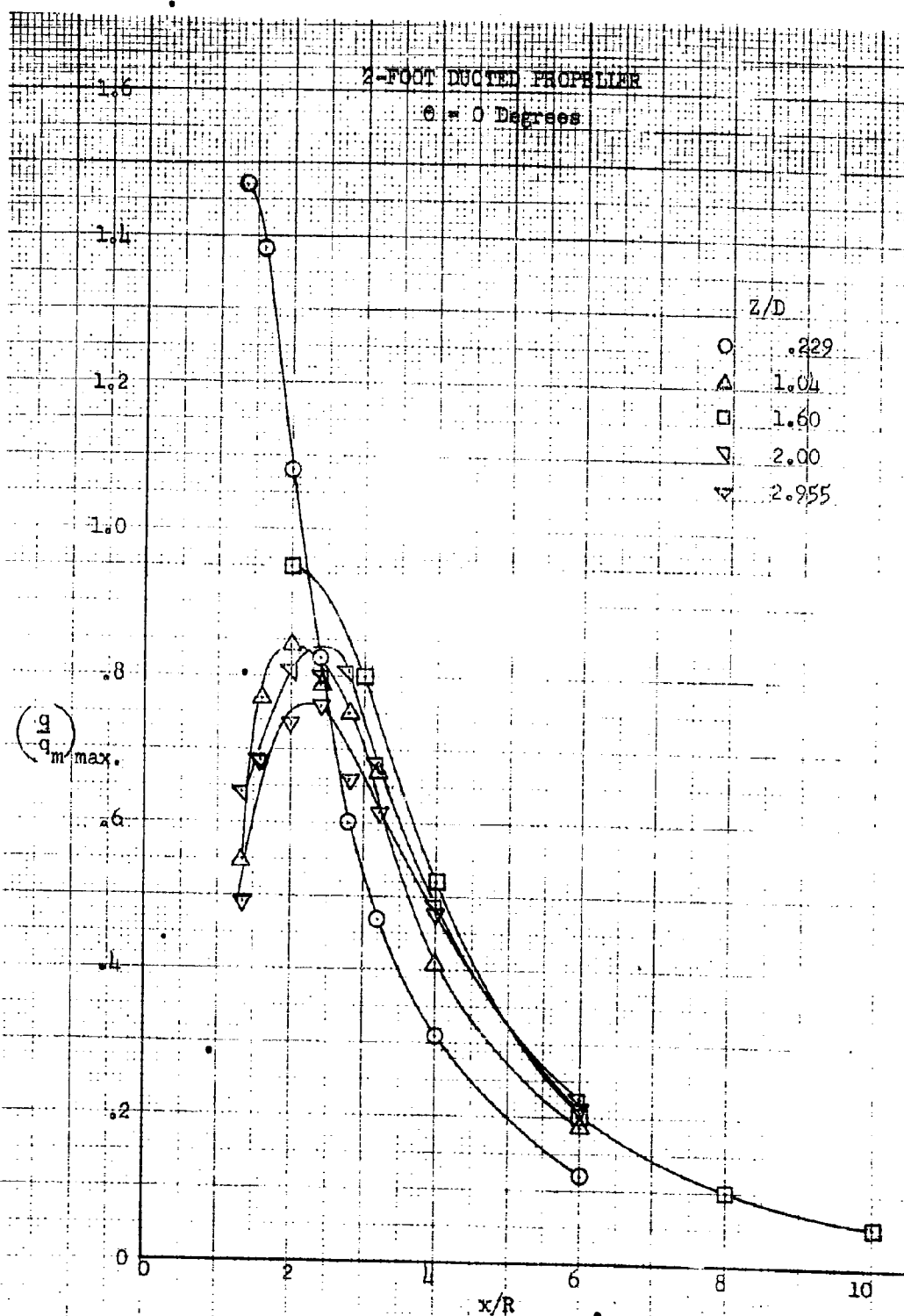


FIGURE 3 VARIATION OF $(q/q_m)_{max}$ WITH x/R

2-FOOT DUCTED PROPELLER

$\theta = 0$ Degrees

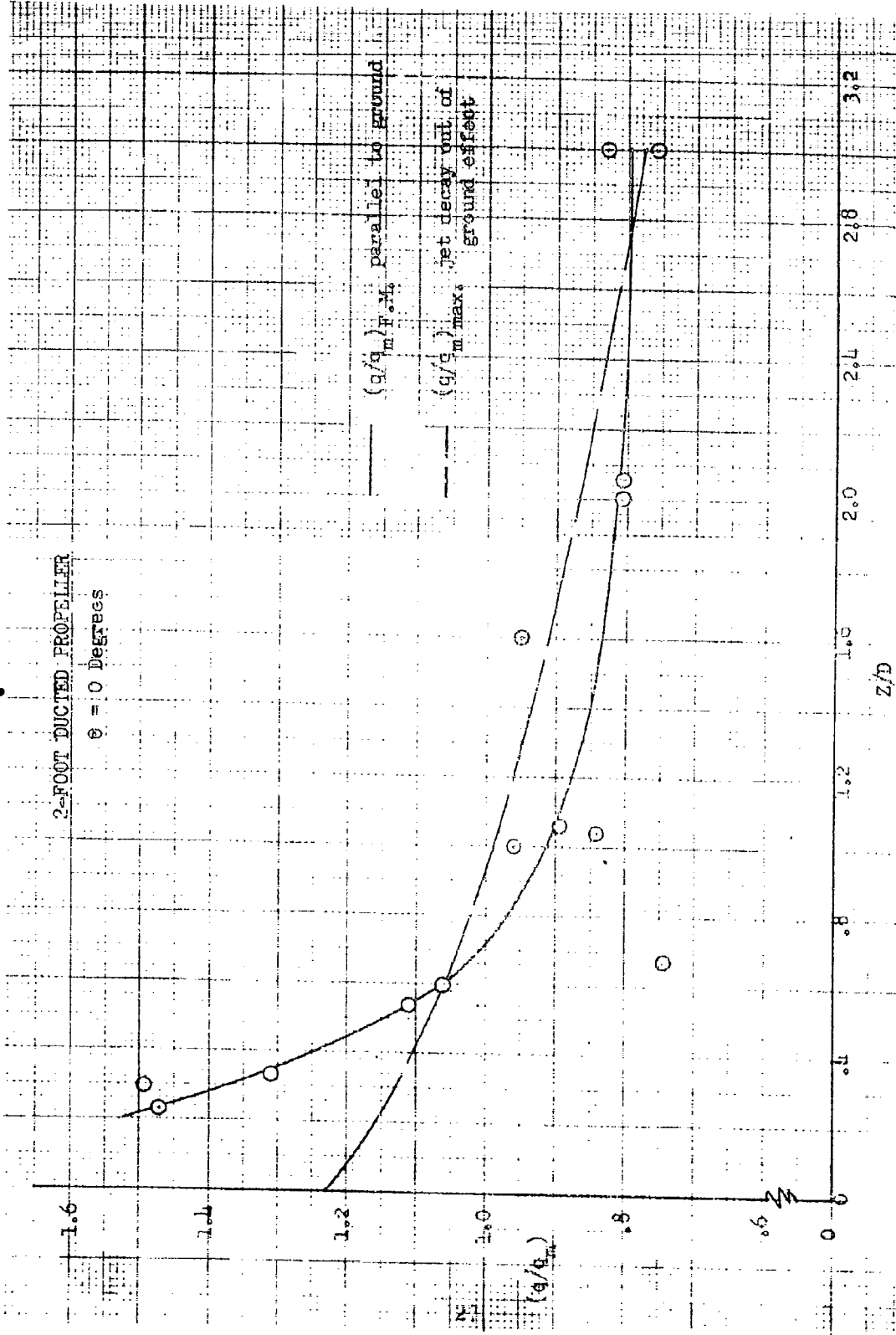


FIGURE 4 FIELD MAXIMUM $(q/q_m)_{F.M.}$ PARALLEL TO GROUND

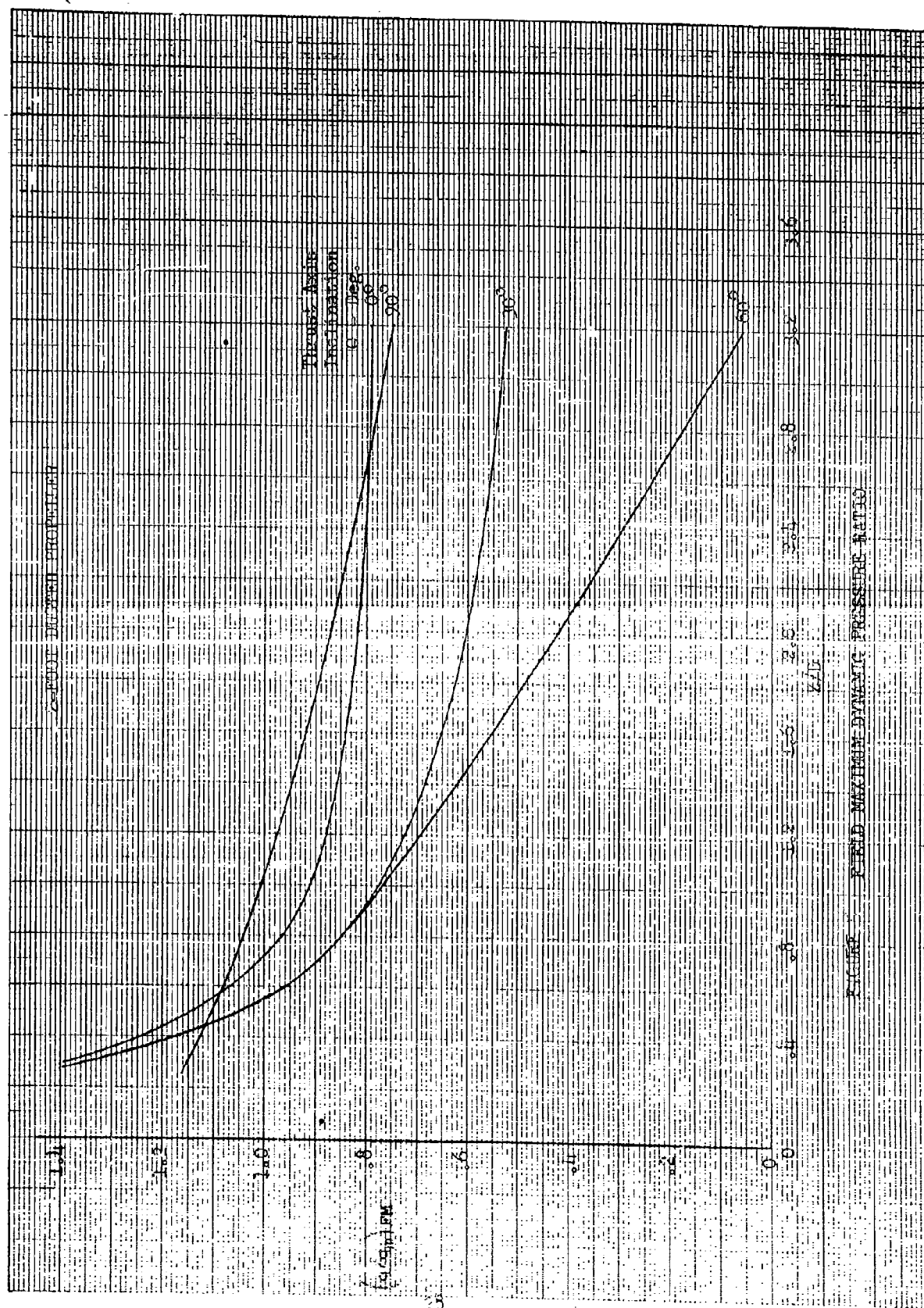


FIGURE FIELD MAXIMUM DYNAMIC PRESSURE RATIO

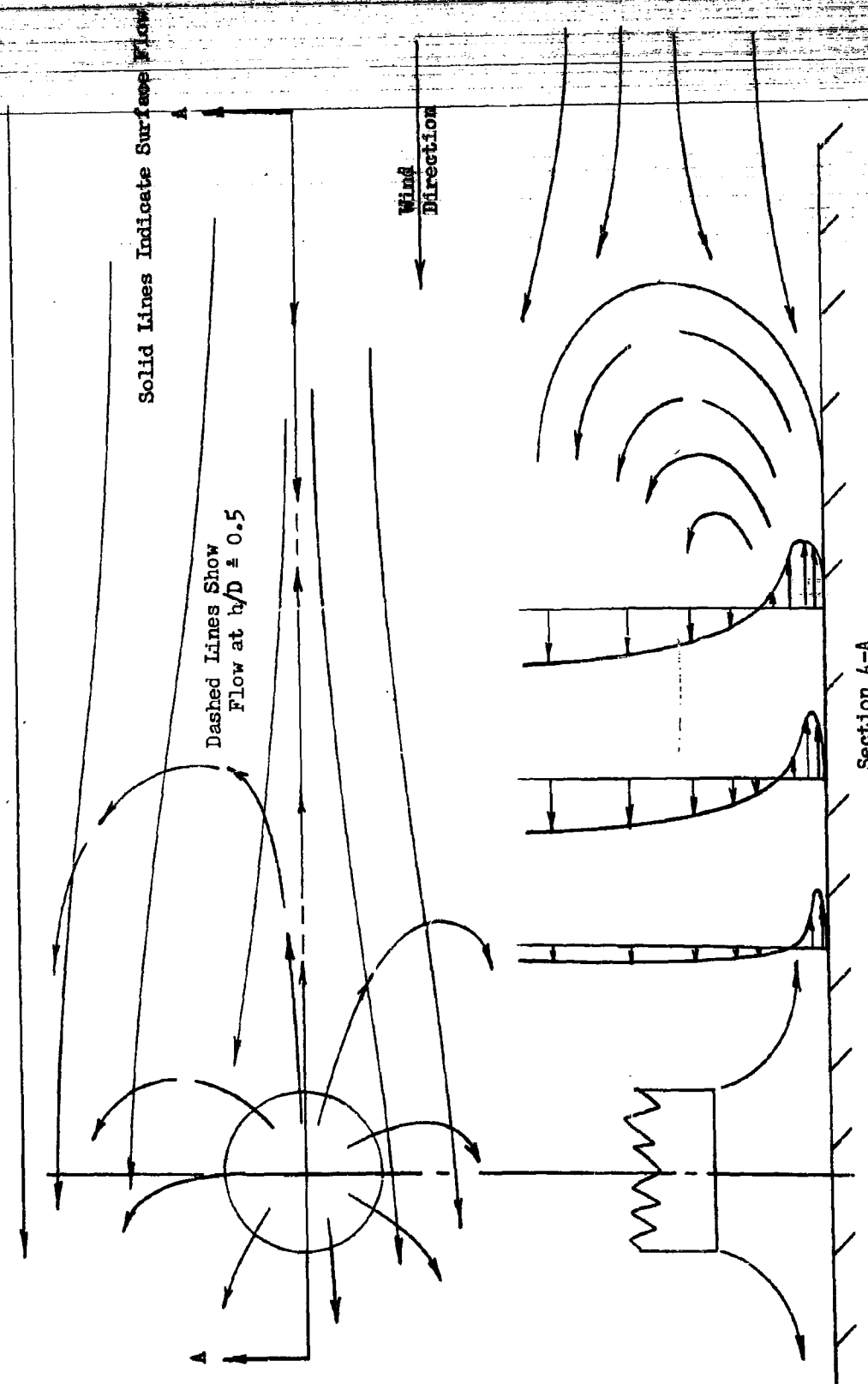


FIGURE 6 INTERACTION BETWEEN JET WAKE AND SURFACE WIND

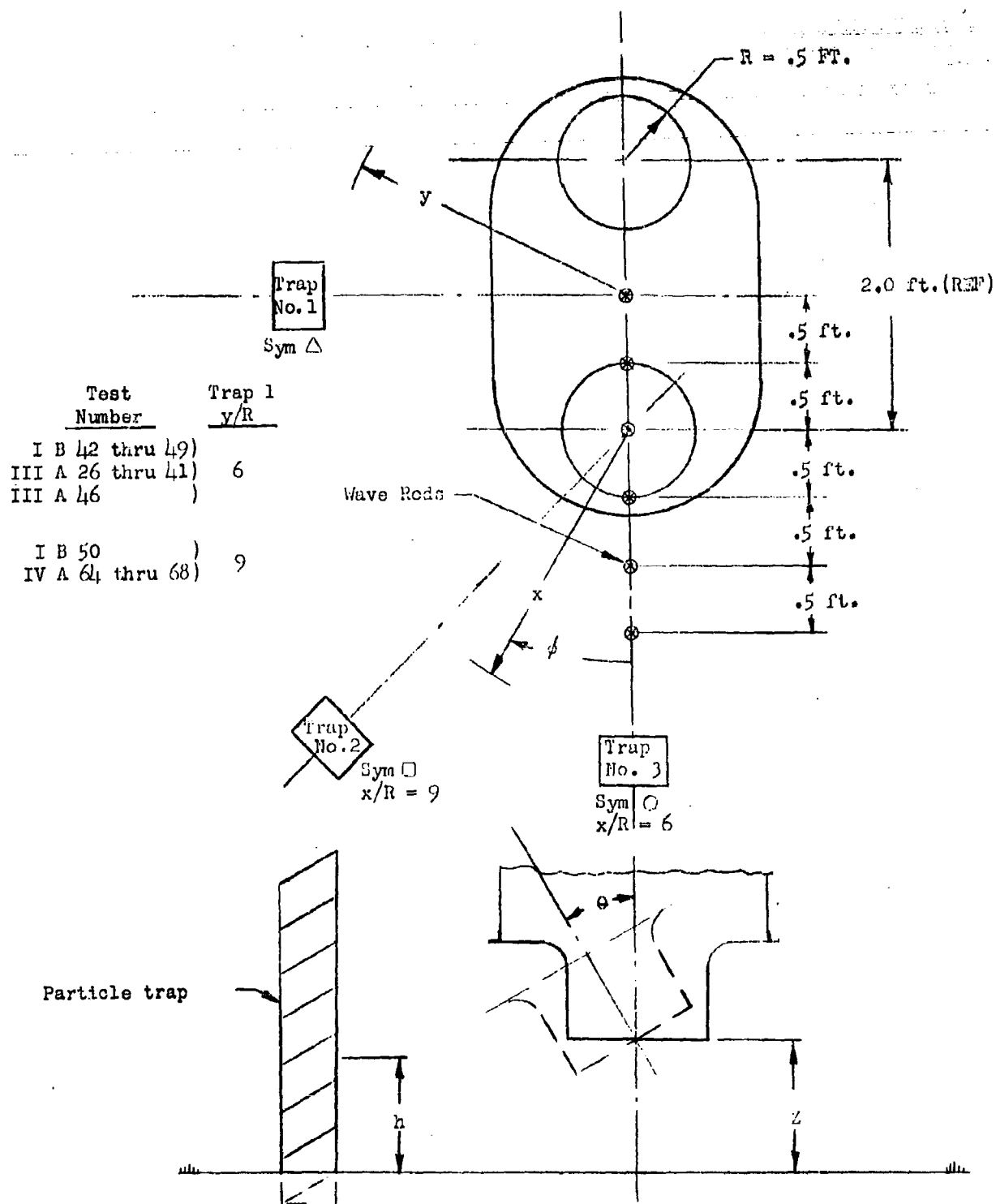


Figure 7 General Arrangement, Test Equipment, Side by Side Flow Adapter

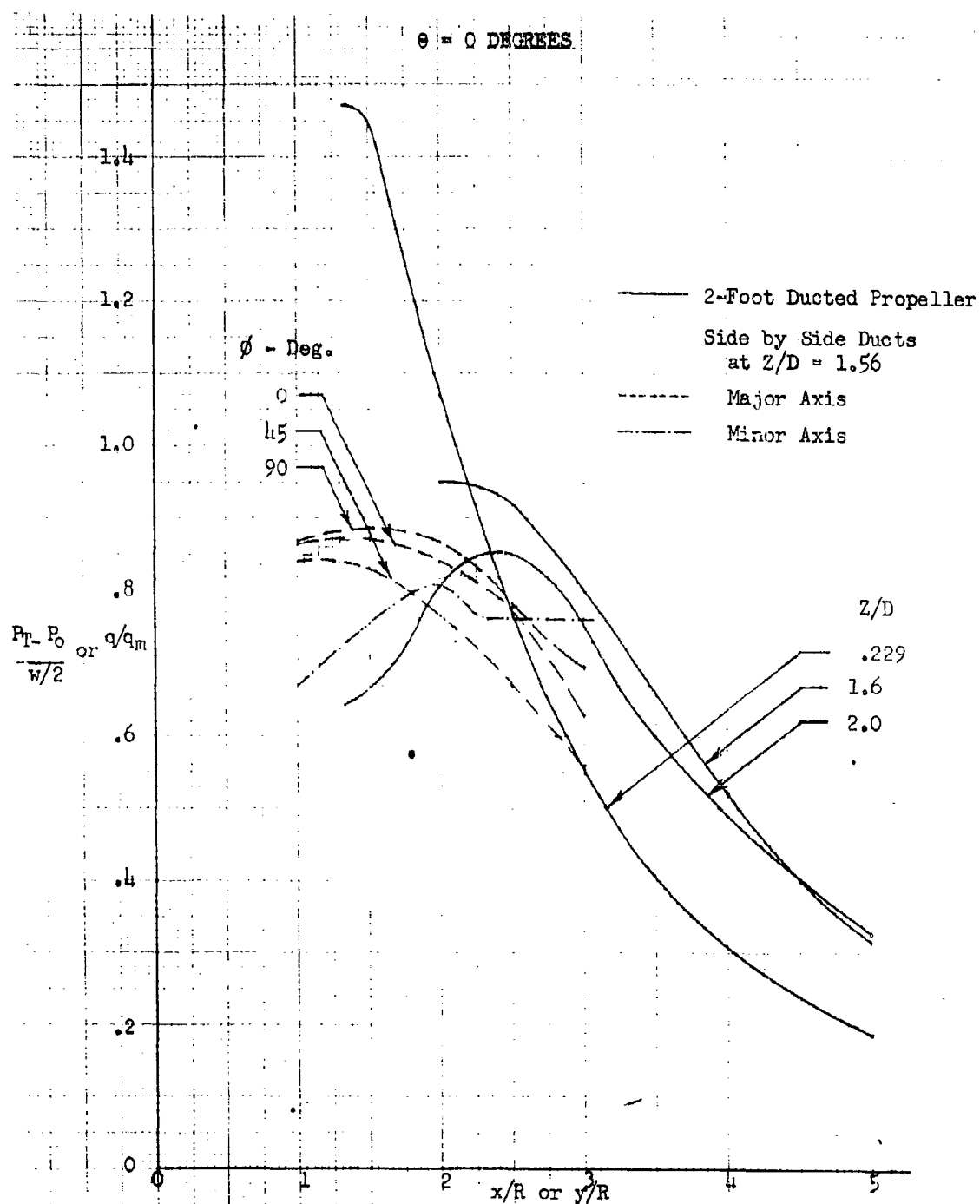


FIGURE 8 DYNAMIC OR TOTAL PRESSURE DECAY

SIDE BY SIDE DUCTS

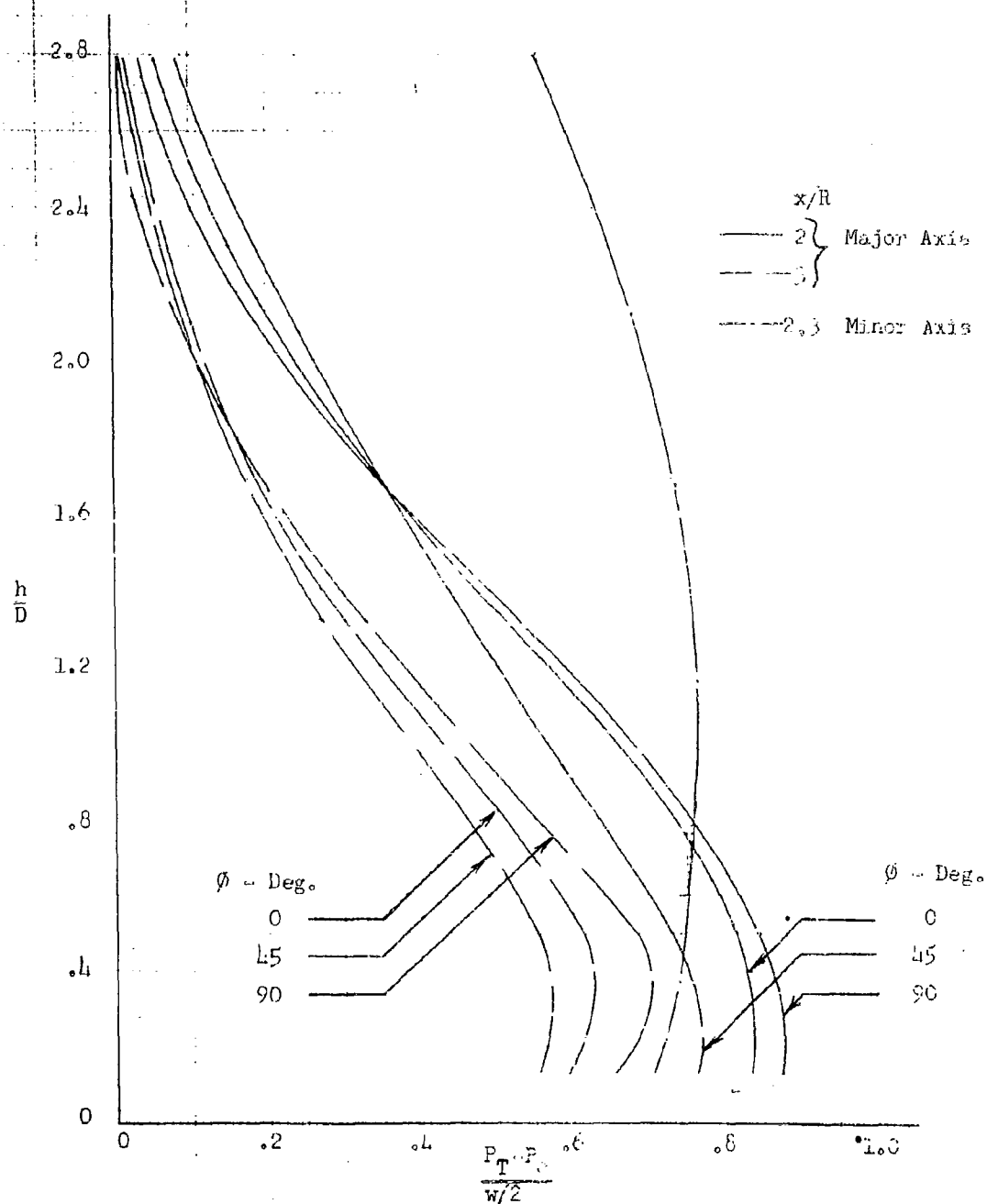
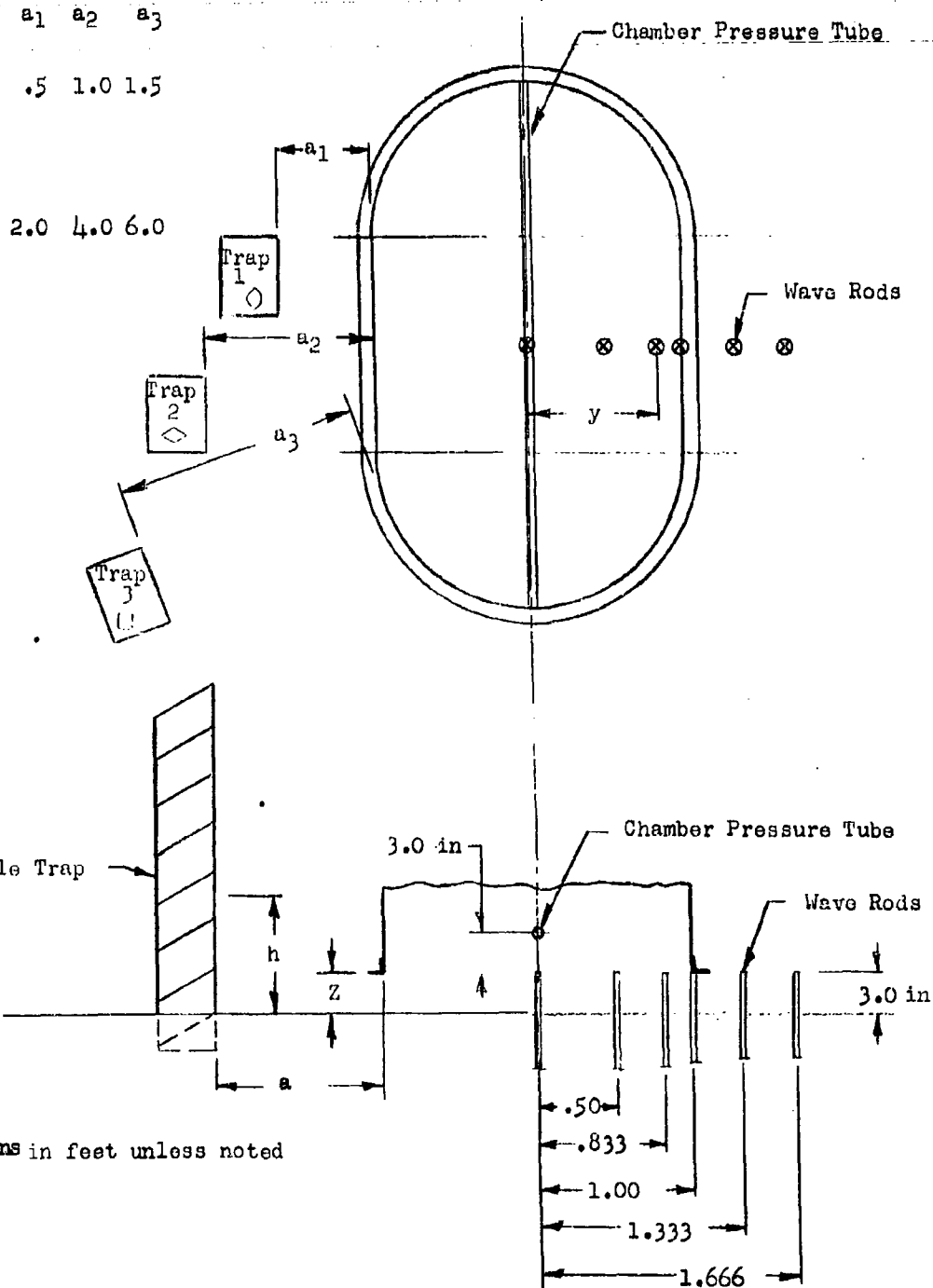


FIGURE 9 TOTAL PRESSURE PROFILES

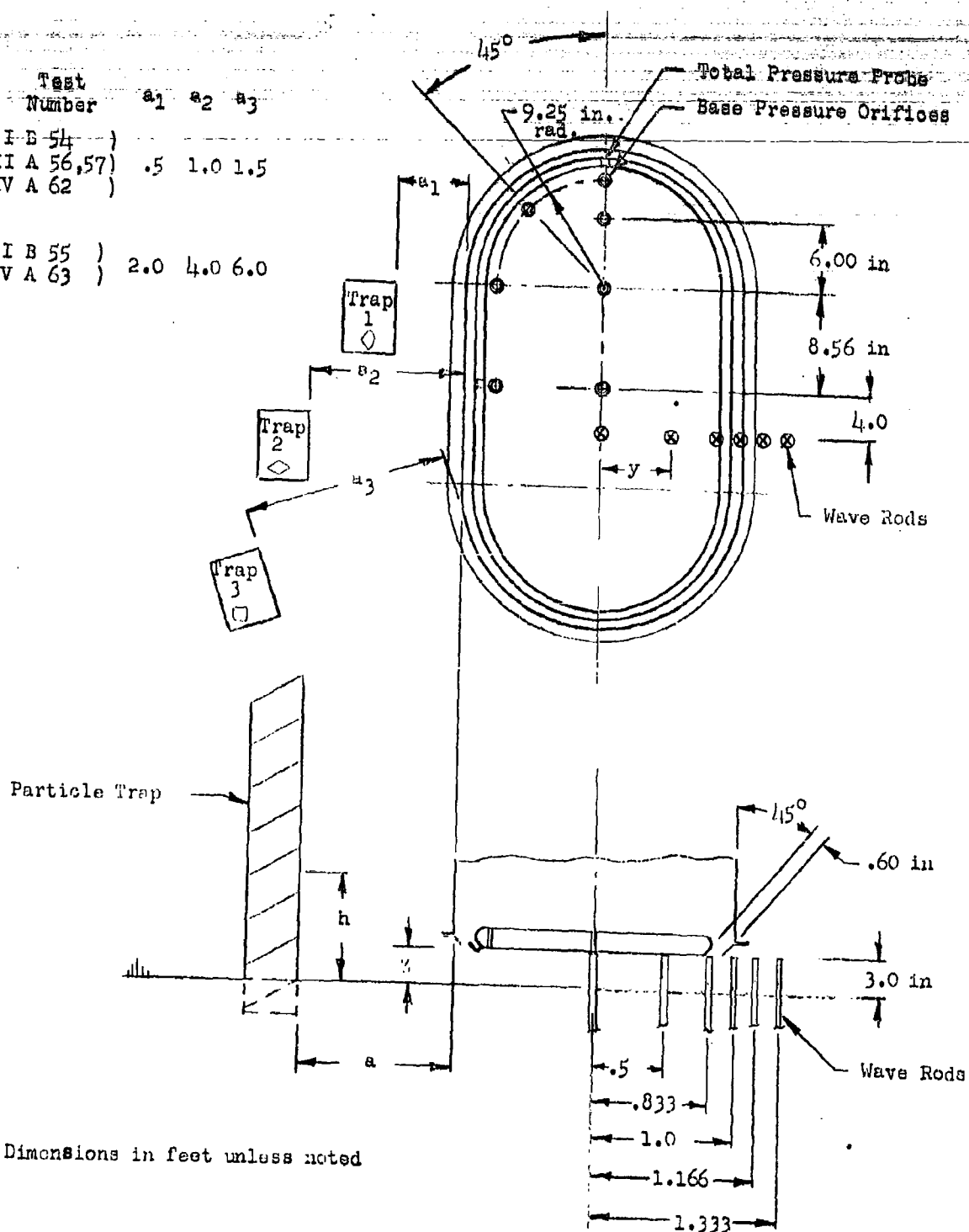
Test Number	a_1	a_2	a_3
I B 52)			
III A 58)	.5	1.0	1.5
IV A 60)			
I B 53)			
III A 59)	2.0	4.0	6.0
IV A 61)			



NOTE: Dimensions in feet unless noted

Figure 10 General Arrangement, Test Equipment
Plenum Chamber

Test Number	a1	a2	a3
IB 54)			
III A 56,57)	.5	1.0	1.5
IV A 62)			
IB 55)			
IV A 63)	2.0	4.0	6.0



NOTE: Dimensions in feet unless noted

Figure 11 General Arrangement, Test Equipment
Annular Nozzle Flow Adapter

SIDE BY SIDE FLOW ADAPTER

(r) Radial Distance (Inches)

(h) Height (Inches)

Soil Condition III A 33, h1 and h6

$z/d = 1.5$

8 Inch Nozzle Length

26 1/2 Inch Nozzle Length

Single 8 Inch Nozzle Length

(One Nozzle Diverted)

Figure 12 Profile of Eroded Sand

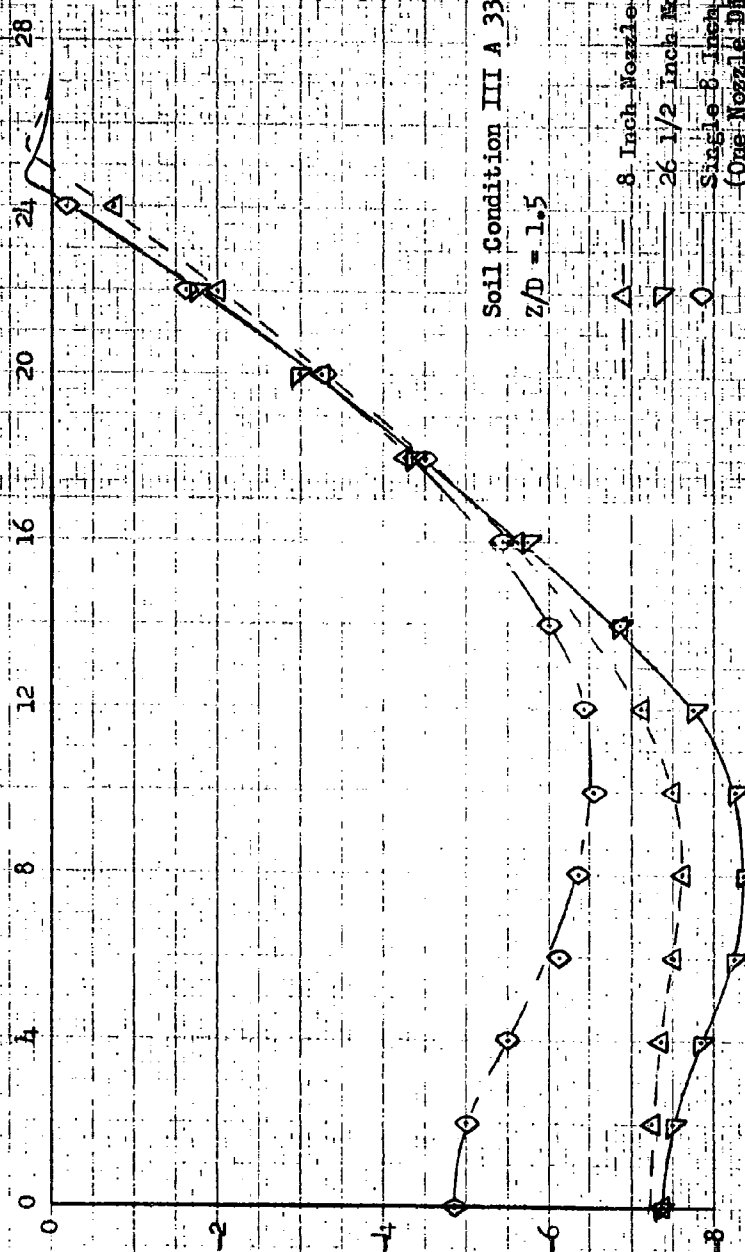
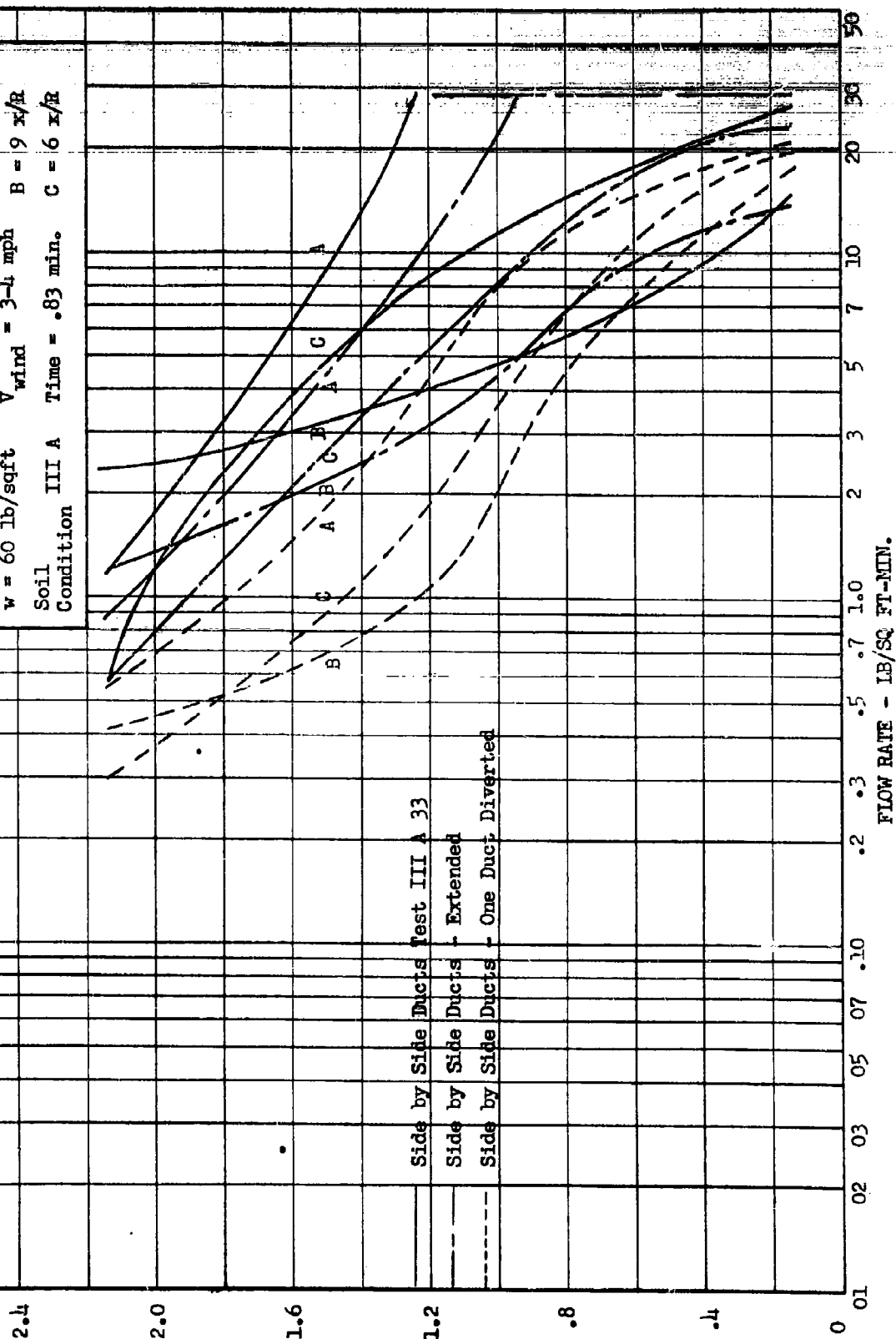




FIG. 13. IMPINGEMENT PATTERN, SIDE BY SIDE FLOW ADAPTER

FIGURE 11: FLOW RATE PROFILES

$Z/D = 1.5$ $\theta = 0$ Deg. $A = 6$ y/r
 $w = 60$ lb/sqft $V_{wind} = 34$ mph $B = 9$ x/r
 Soil III A Time = .83 min. $C = 6$ x/r
 Condition



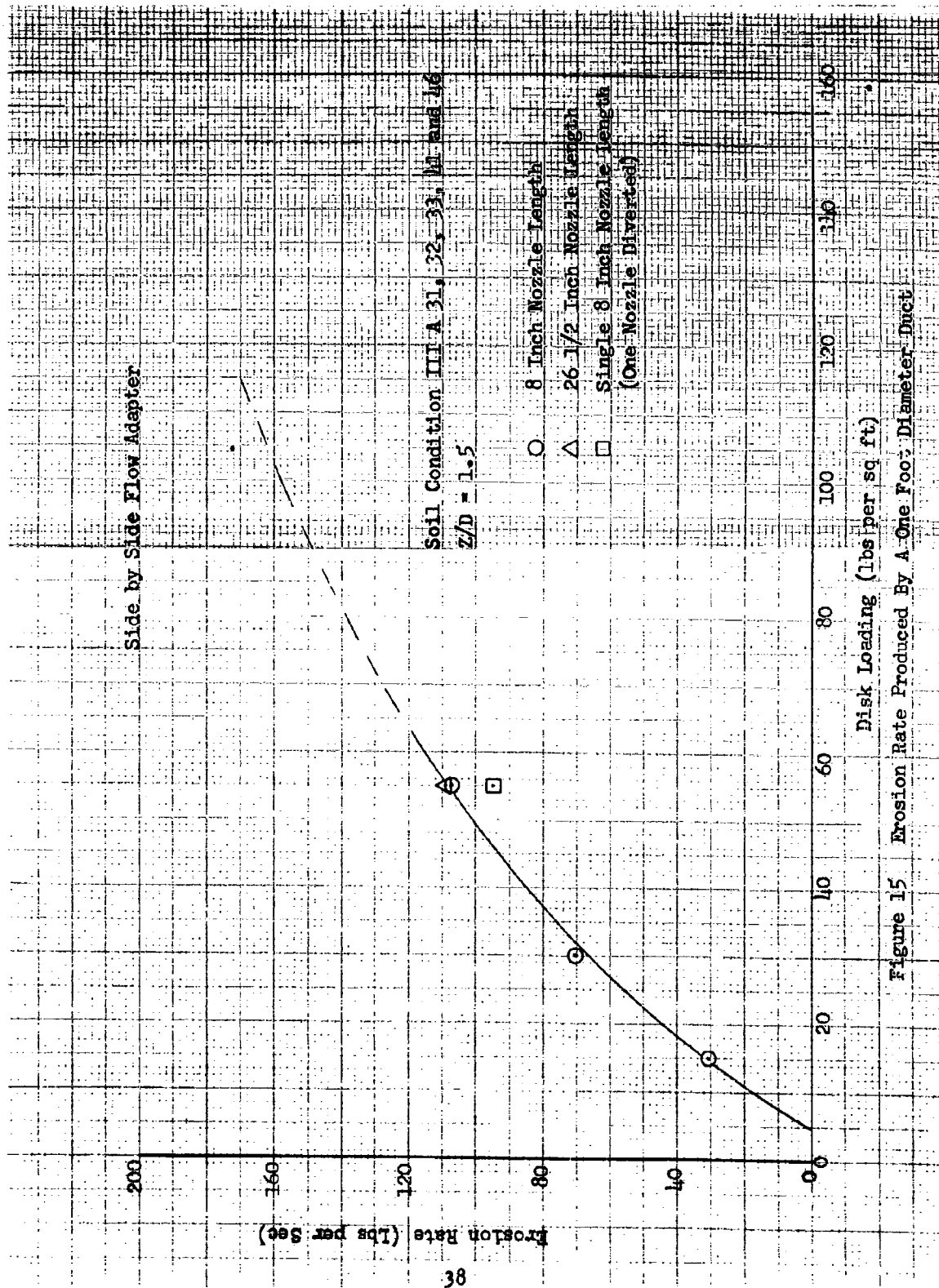


Figure 15 Erosion Rate Produced By A One Foot Diameter Duct

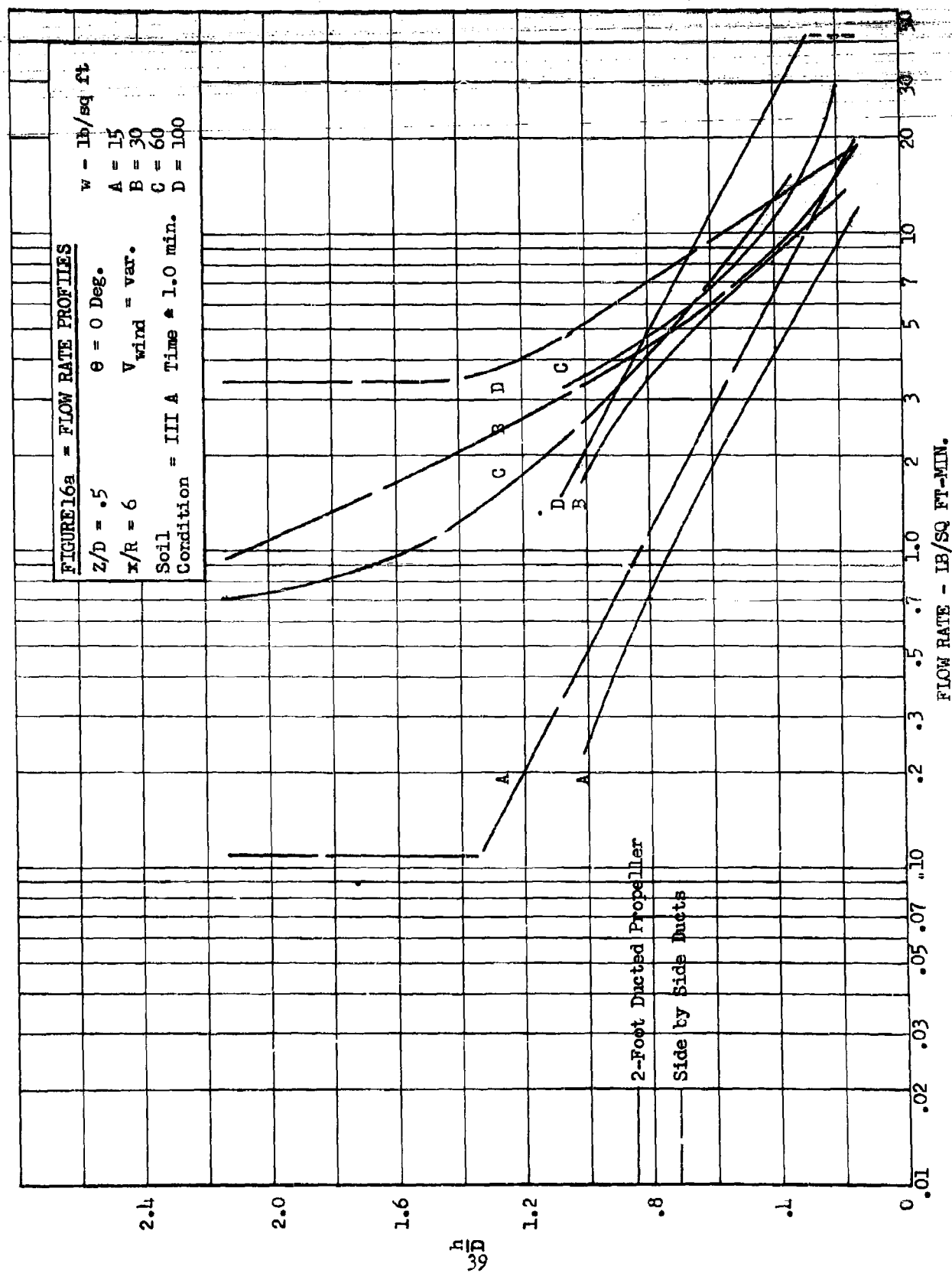


FIGURE 16b: FLOW RATE PROFILES

w - lb/sq ft.

A = 15

B = 30

C = 60

D = 100

$\theta = 0$ Deg.

$V_{wind} = \text{var.}$

Soil Condition = III A Time = 1.0 min.

D = 100

$z/d = .5$

$x/r = 9$

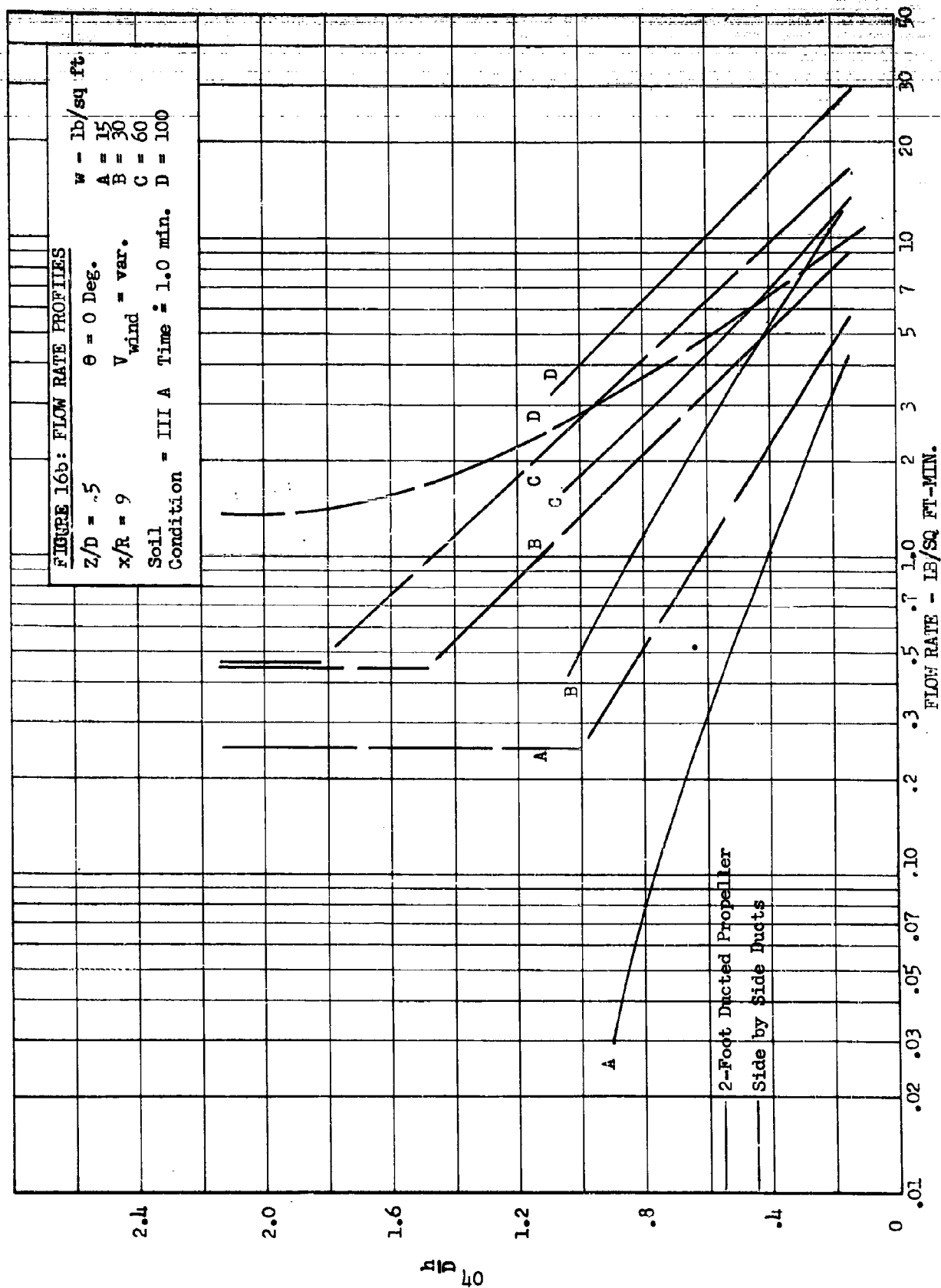
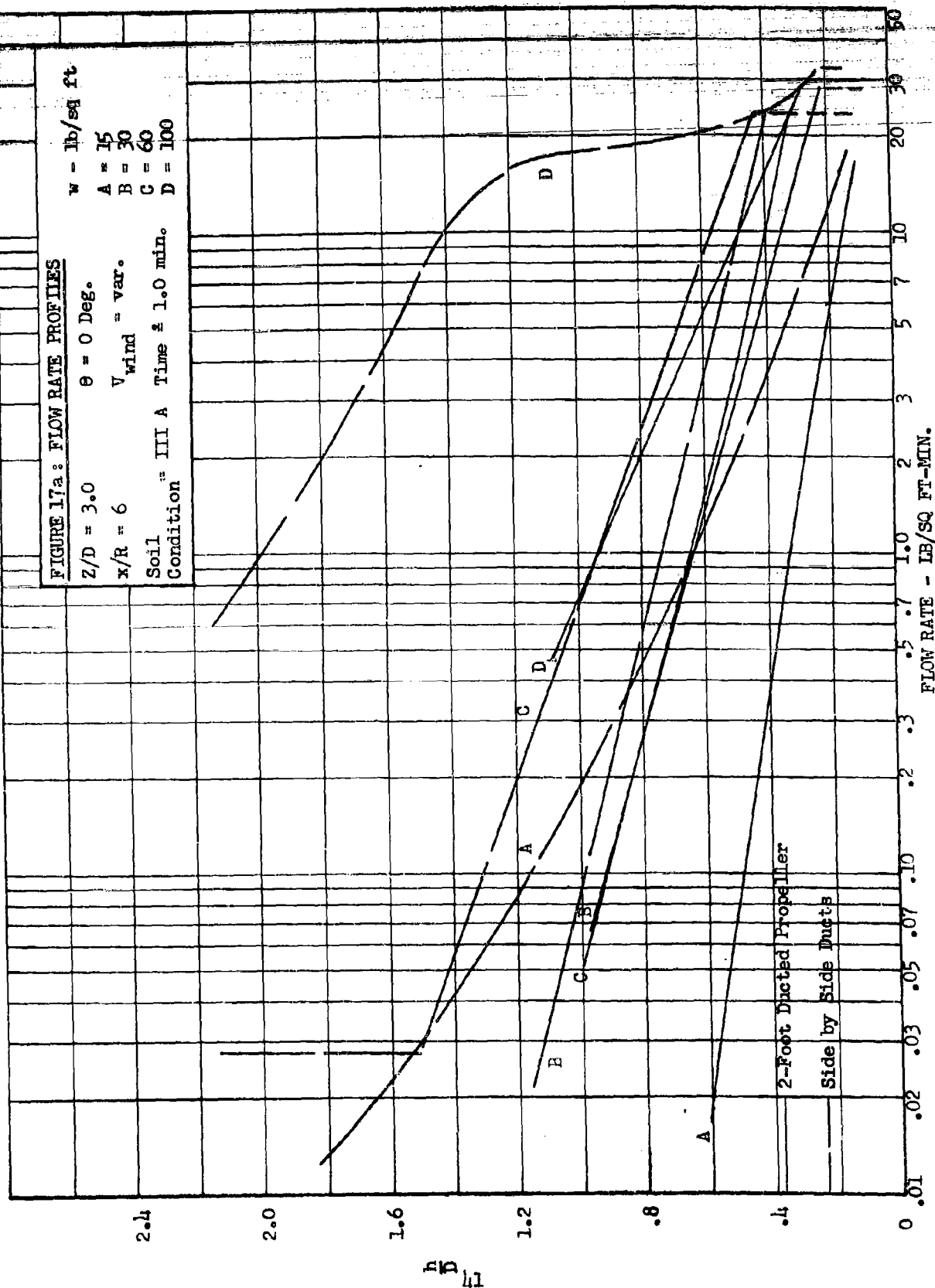


FIGURE 17a: FLOW RATE PROFILES

$w = \text{lb/sq ft}$
 $Z/D = 3.0$ $\theta = 0 \text{ Deg.}$
 $x/R = 6$ $V_{\text{wind}} = \text{var.}$
 Soil Condition = III A Time $\pm 1.0 \text{ min.}$
 $A = 15$
 $B = 30$
 $C = 60$
 $D = 100$



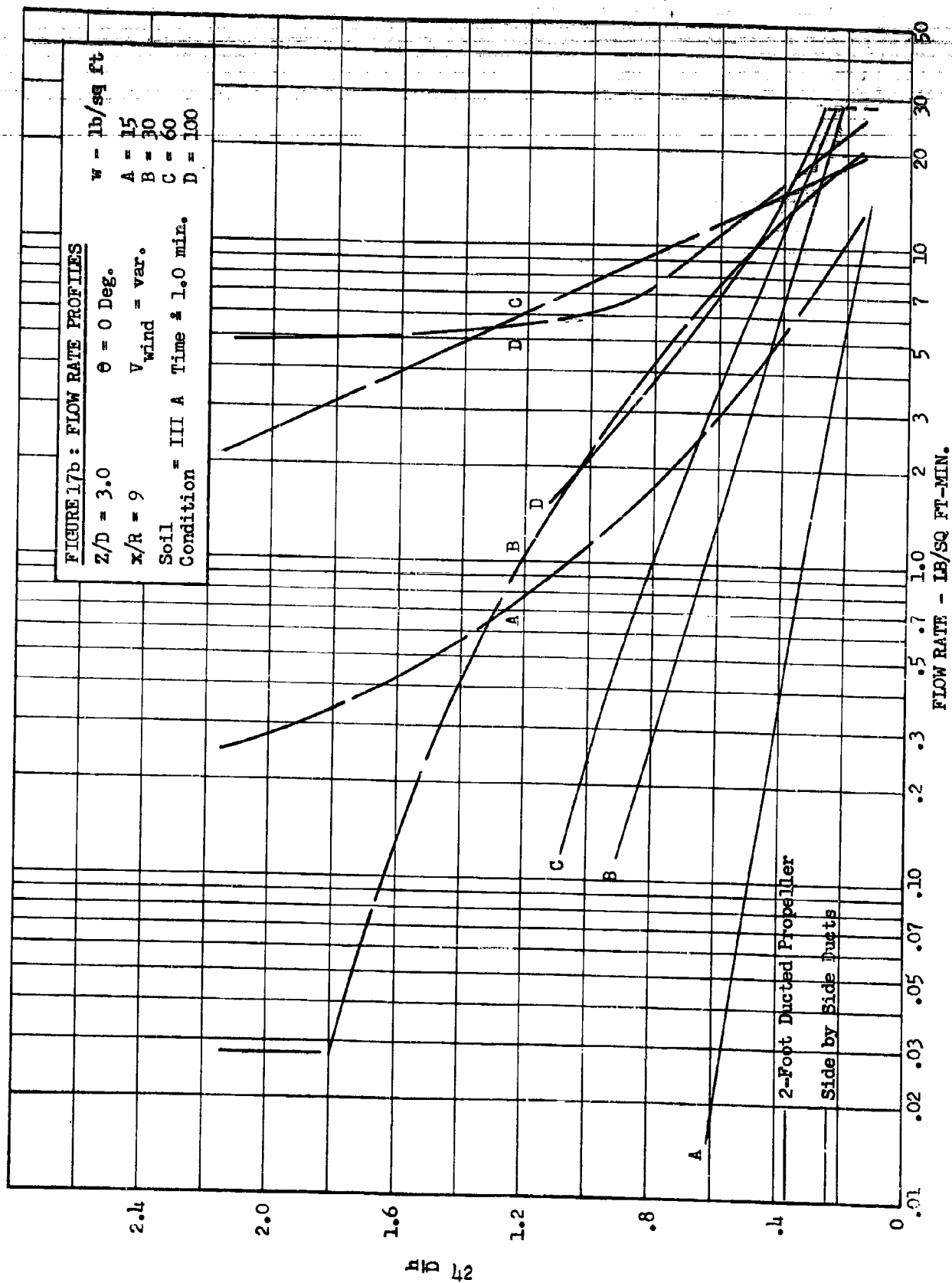
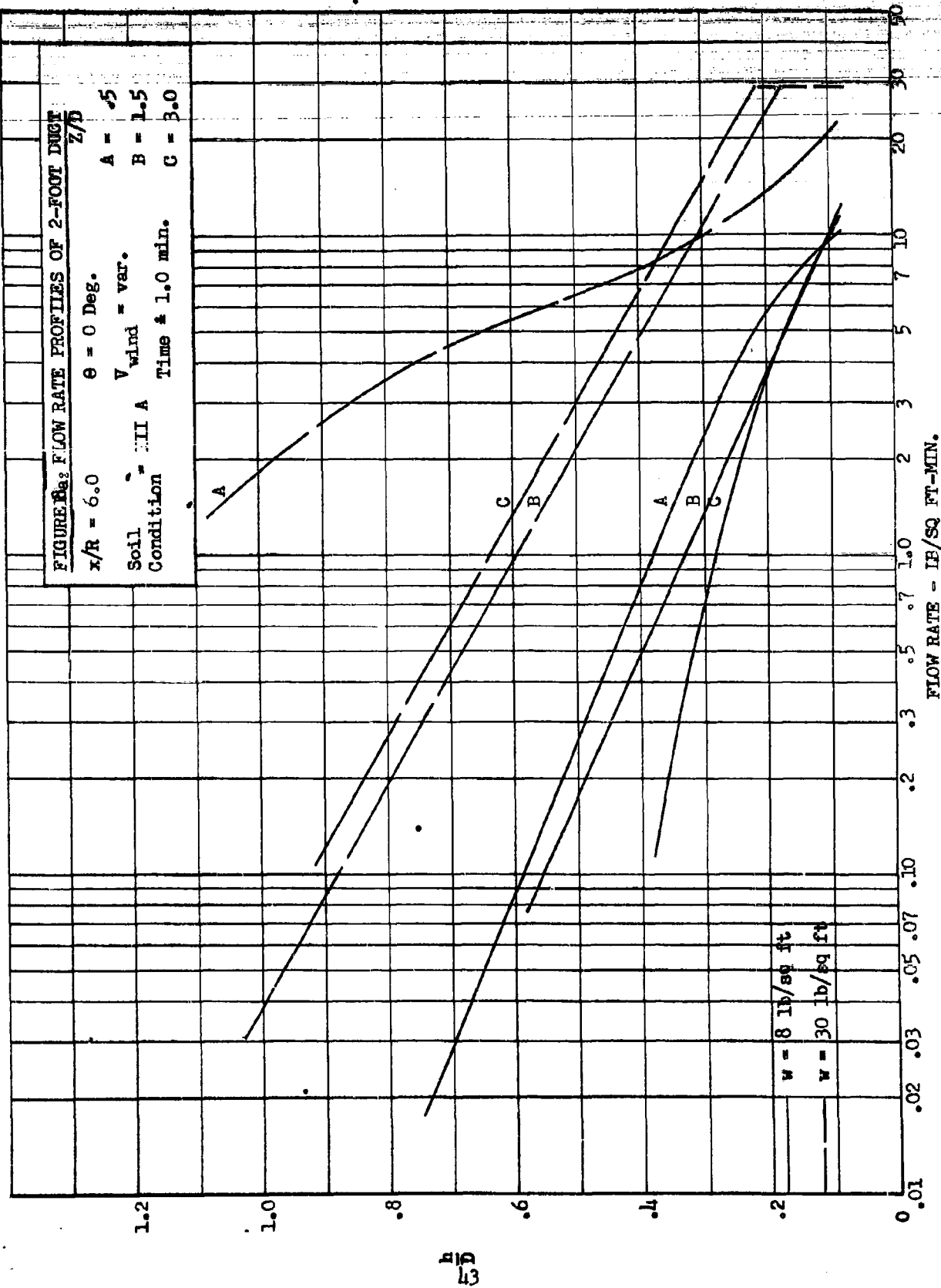
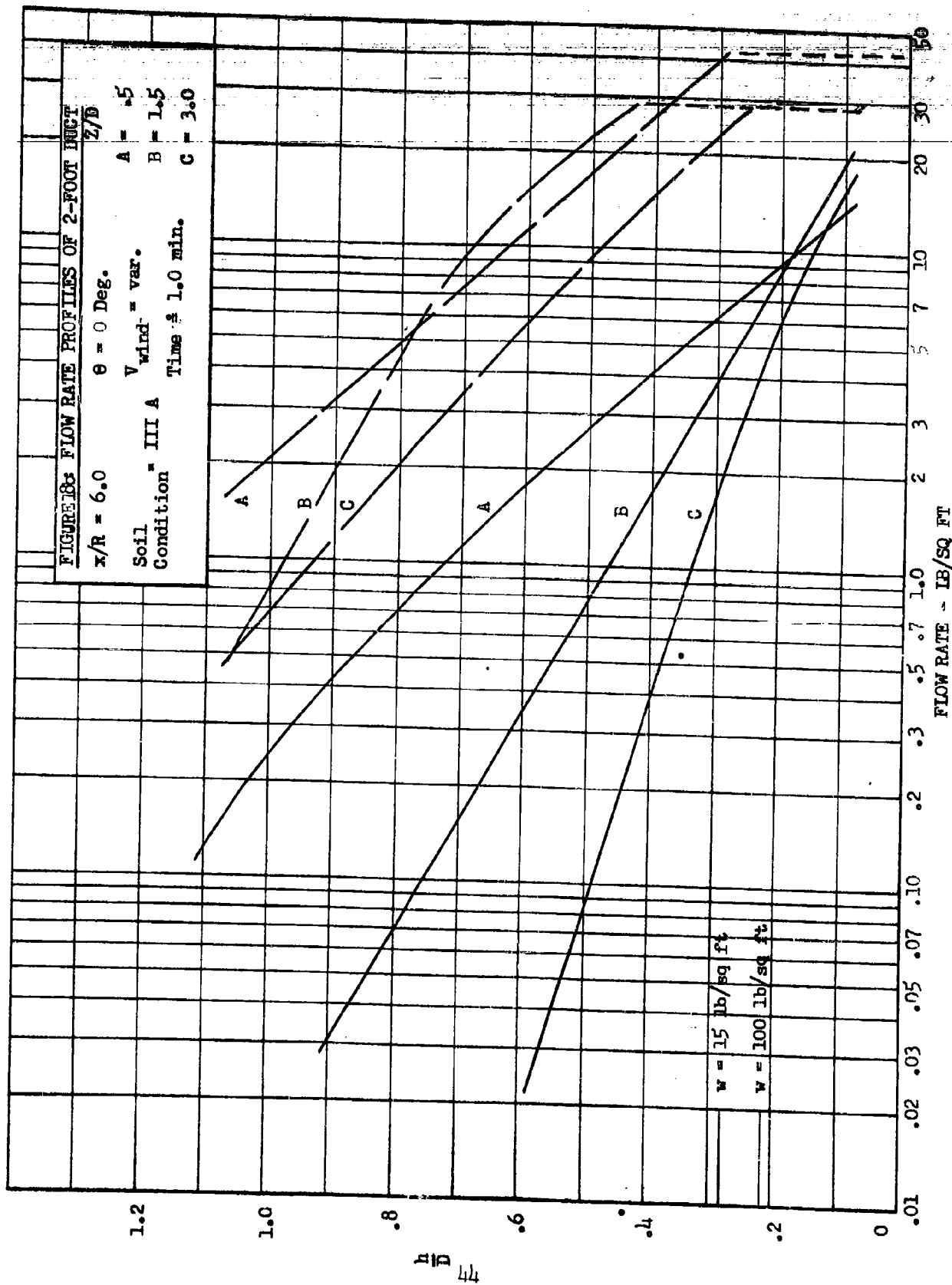


FIGURE 8a: FLOW RATE PROFILES OF 2-FOOT DIRT

$x/R = 6.0$ $\theta = 0$ Deg. $A = .5$
 z/D
 Soil Condition III A $V_{wind} = \text{var.}$ $B = 1.5$
 Time ± 1.0 min. $C = 3.0$





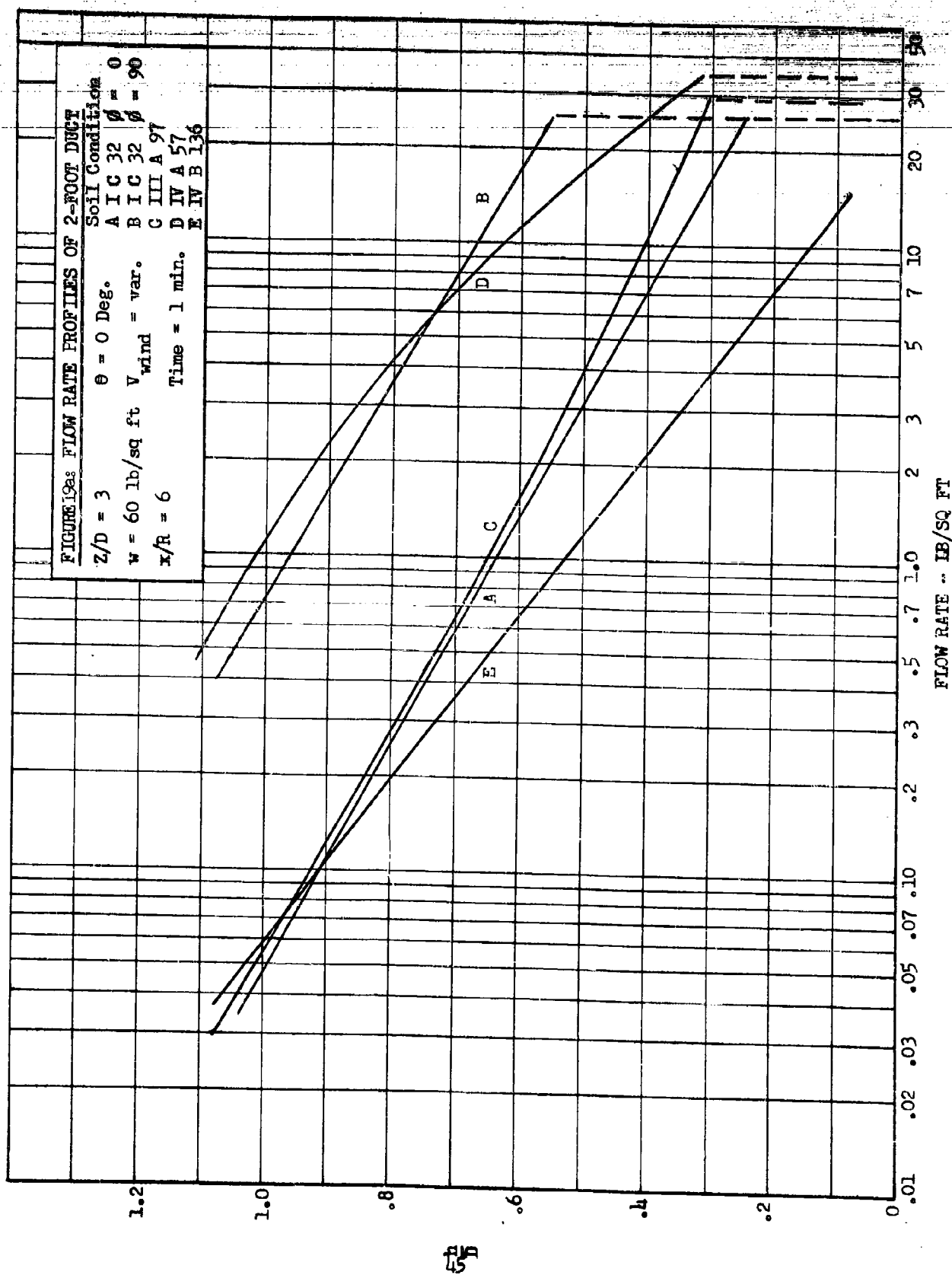


FIGURE 9b: FLOW RATE PROFILES - SIDE BY SIDE DUCTS

$$z/\eta = 3 \quad \theta = 0 \text{ Deg.} \quad \text{Soil Condition}$$

W = 60 lb/sq ft V = var. A = I B 43

$\gamma/P = 6$ $B = III$ A 38

Time = 1 min.

49 AT = 3

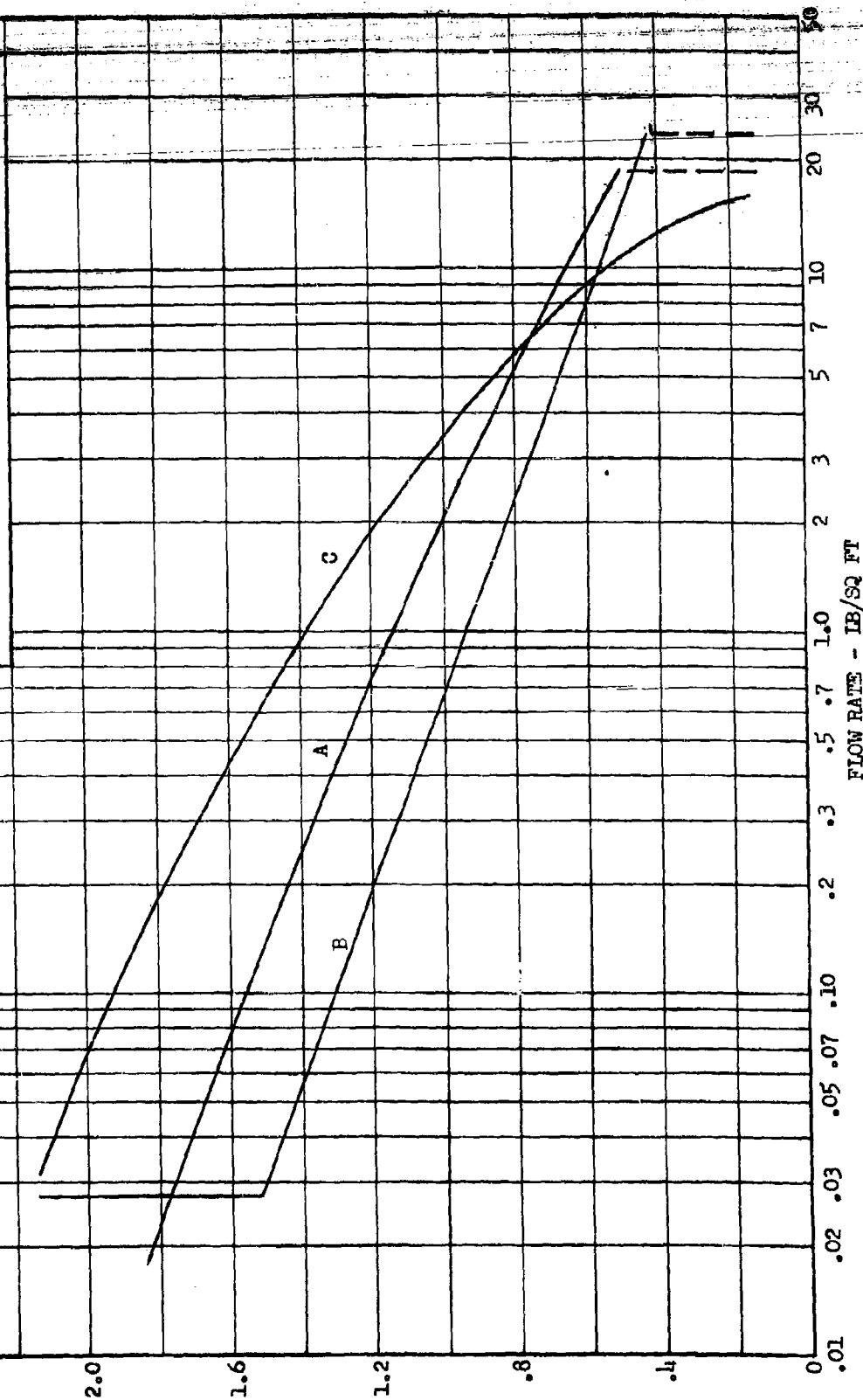
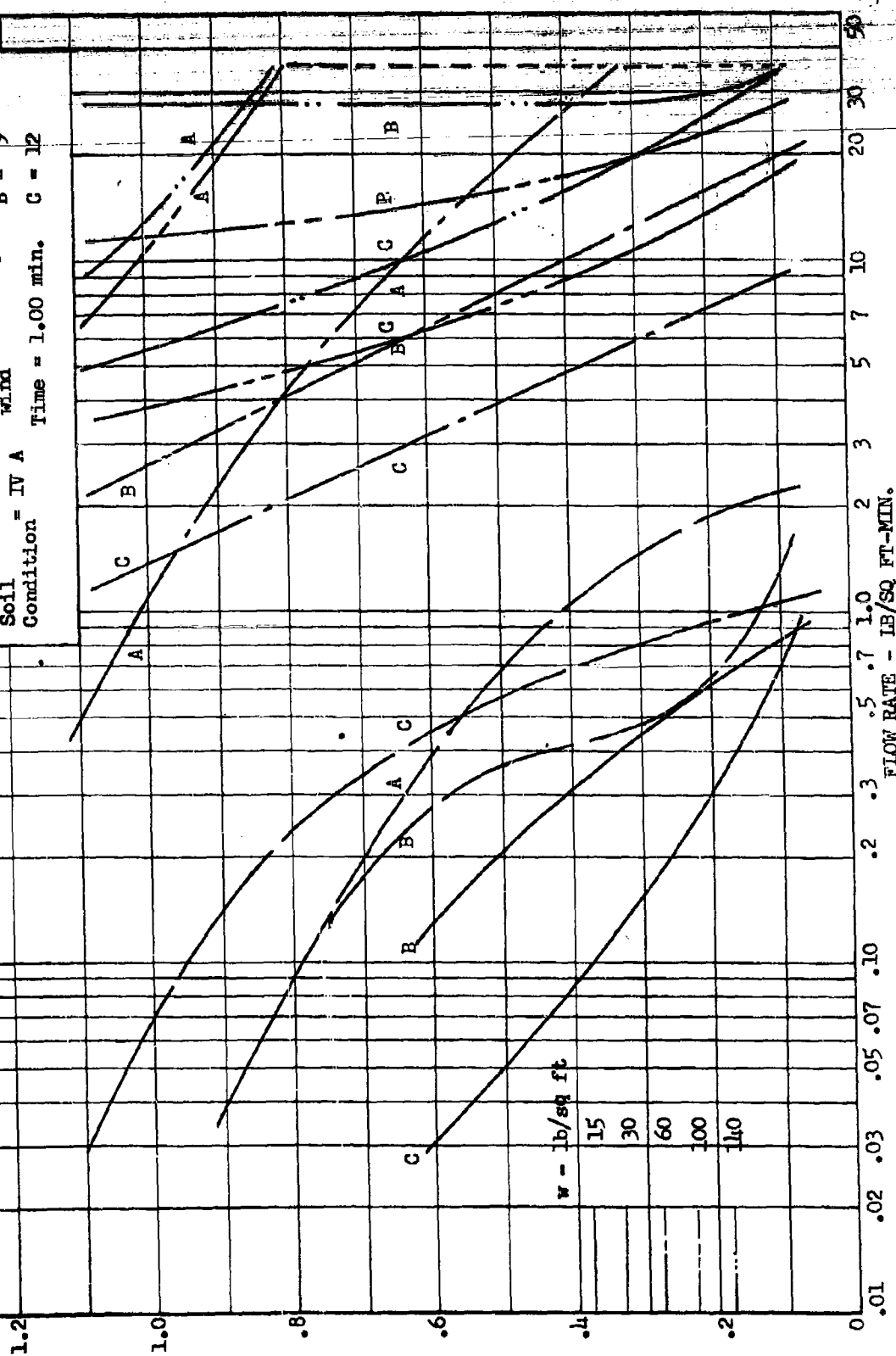


FIGURE 2 FLOW RATE PROFILES 2-FOOT DUCT

$Z/D = 3$ $\theta = 0$ Deg. x/H
 $A = 6$
 $V_{wind} = 6-10$ mph $B = 9$
 $Soil$ Condition = IV A $C = 12$
 $Time = 1.00$ min.



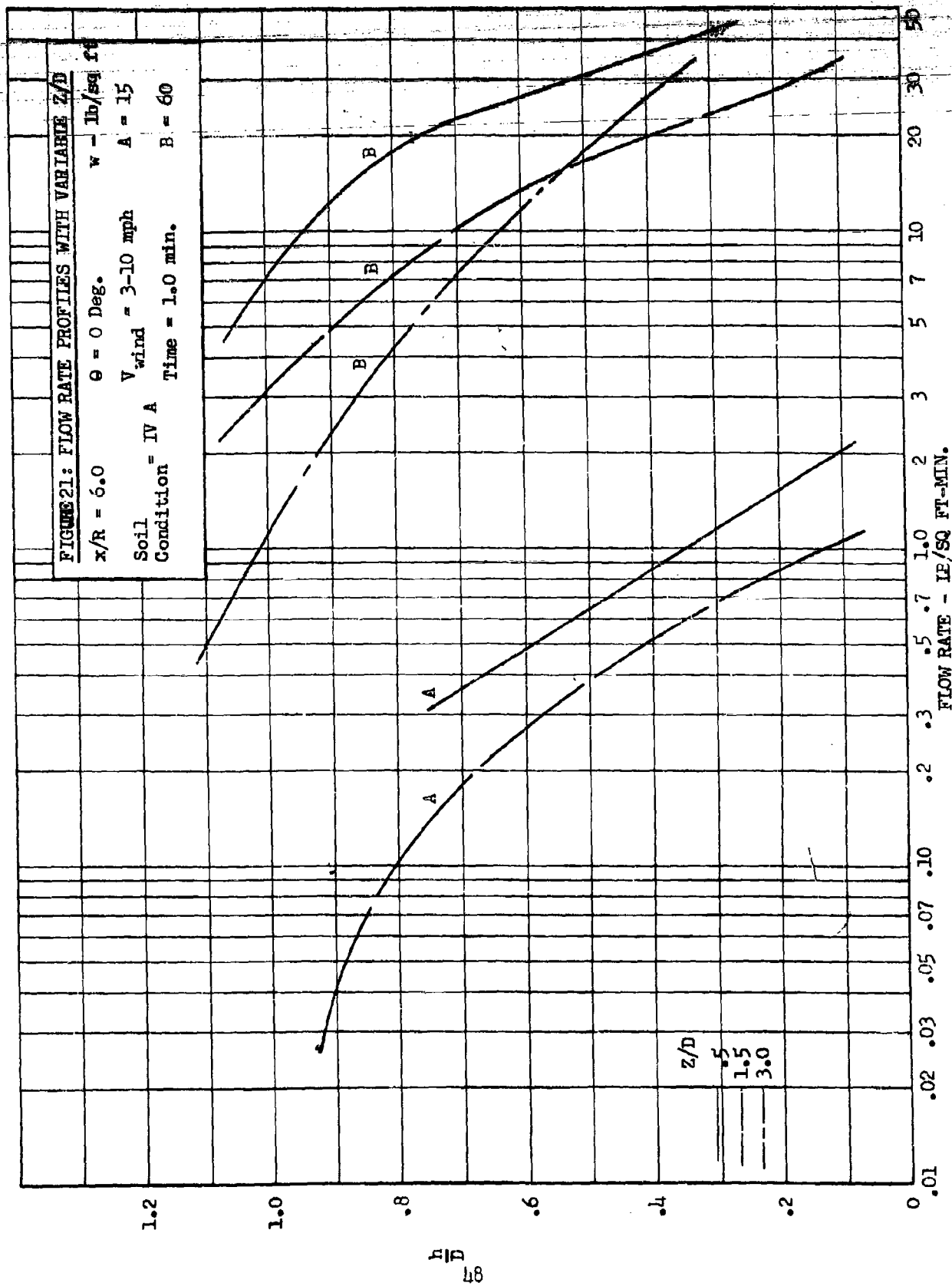


FIGURE 23 FLOW RATE PROFILES COMPARING SOILS
IV A AND IV B

$x/R = 6$ $\theta = 0$ Deg.
 $Z/D = 1.5$ $V_{wind} = 0-8$ mph
 Time = 1.0 min.

Soil Conditions
 A IV A
 B IV B

1.2

1.0

.8

.6

.4

.2

0

$\frac{h}{4.9D}$

w , lb/sq ft

15

30

100

.01

.02

.03

.05

.07

.10

.2

.3

.5

.7

1.0

2

3

5

7

10

20

30

40

FLOW RATE - LB/SQ FT-MIN.

2-FOOT DIAMETER DUCTED PROPELLER

$Z/D = 1.5$

$\theta = 0$ Deg.

$x/R = 6$

Wind = var.

Time = 1.0 min.

Soil Condition

A IV A

B IV B

w - lb/sq ft

15

30

100

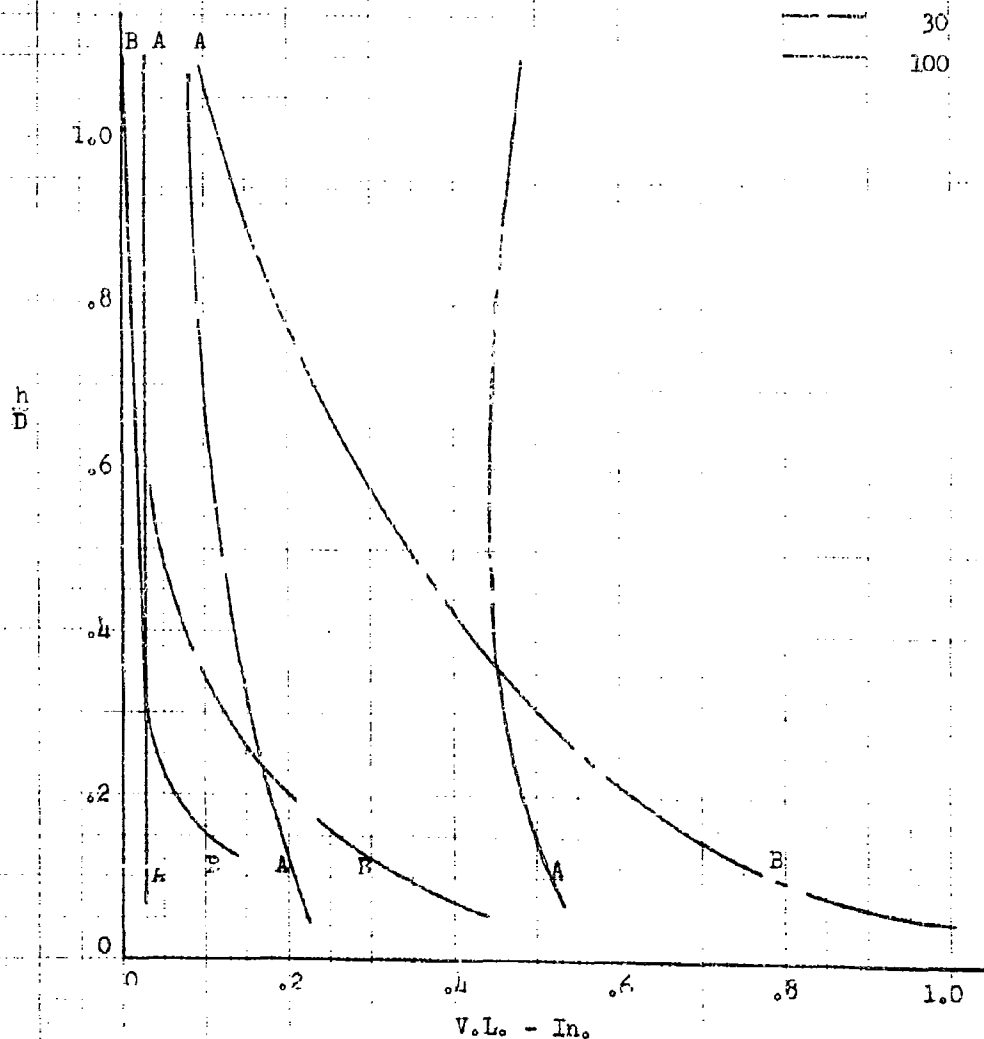


FIGURE 23 PARTICLE SIZE DISTRIBUTION

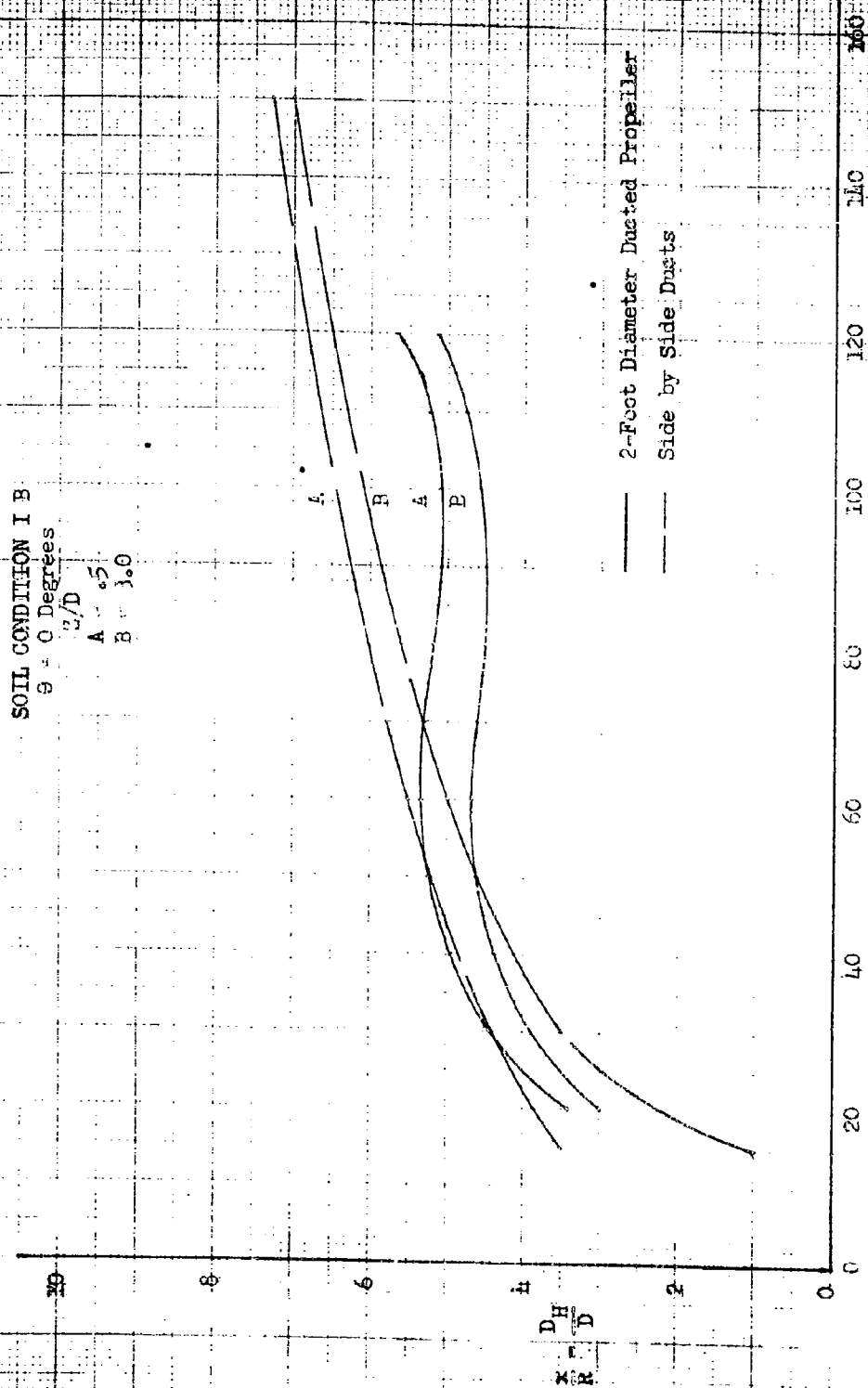
SOIL CONDITION I B

$\theta = 0$ Degrees

u/D

A = .5

B = 1.0



$w = 16$ sq ft.

FIGURE 24 RELATIVE DIAMETER OF ERODED SECTION

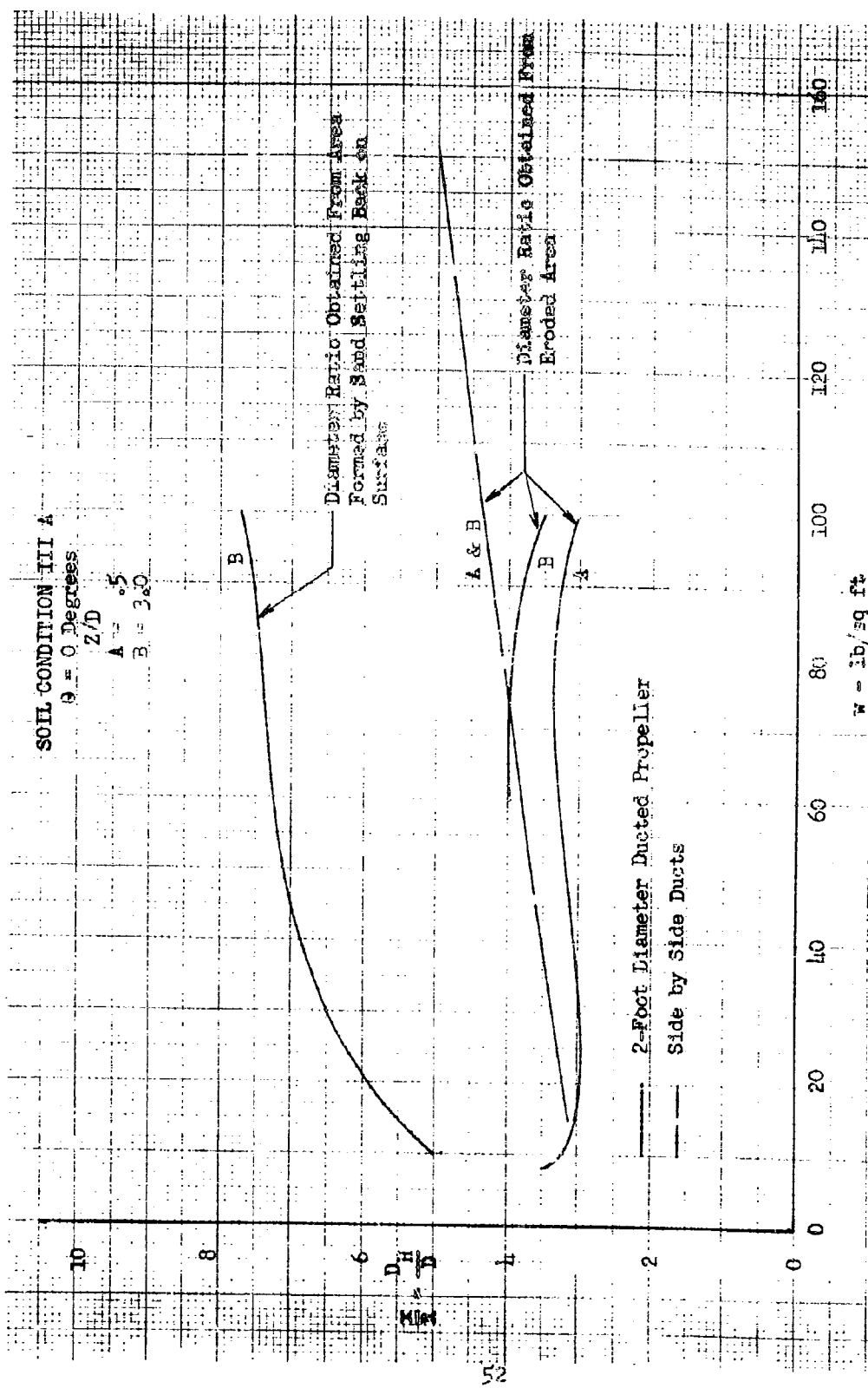


FIGURE 25 RELATIVE DIAMETER OF ERODED SECTION

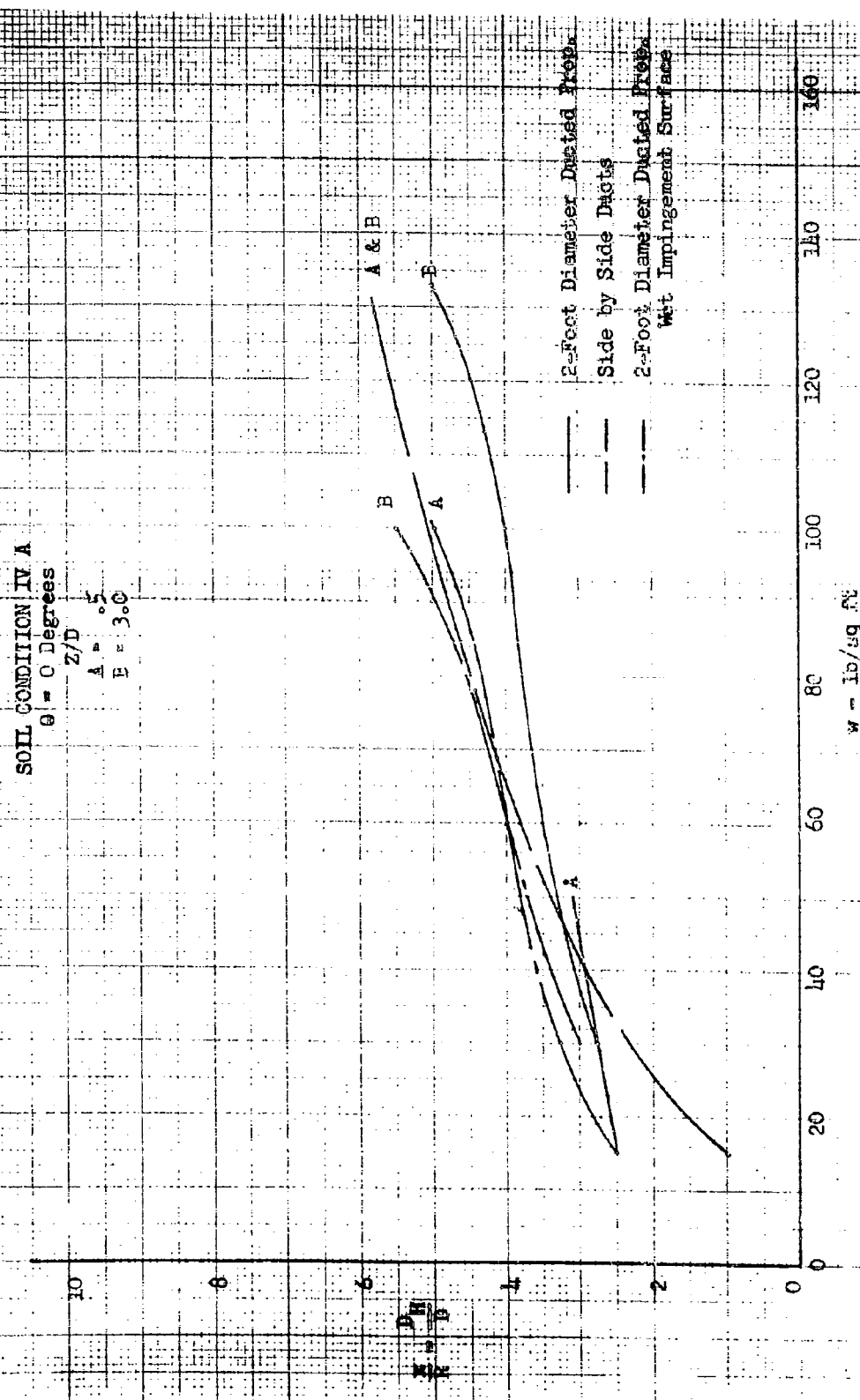


FIGURE 26 RELATIVE DIAMETER OF ERODED SECTION

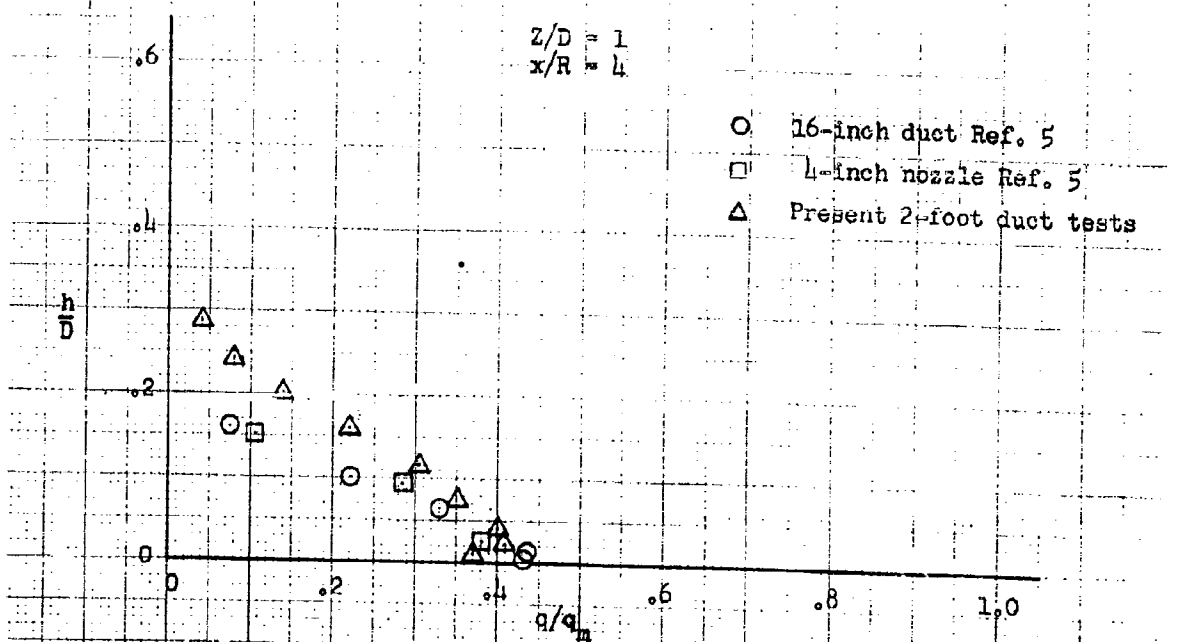
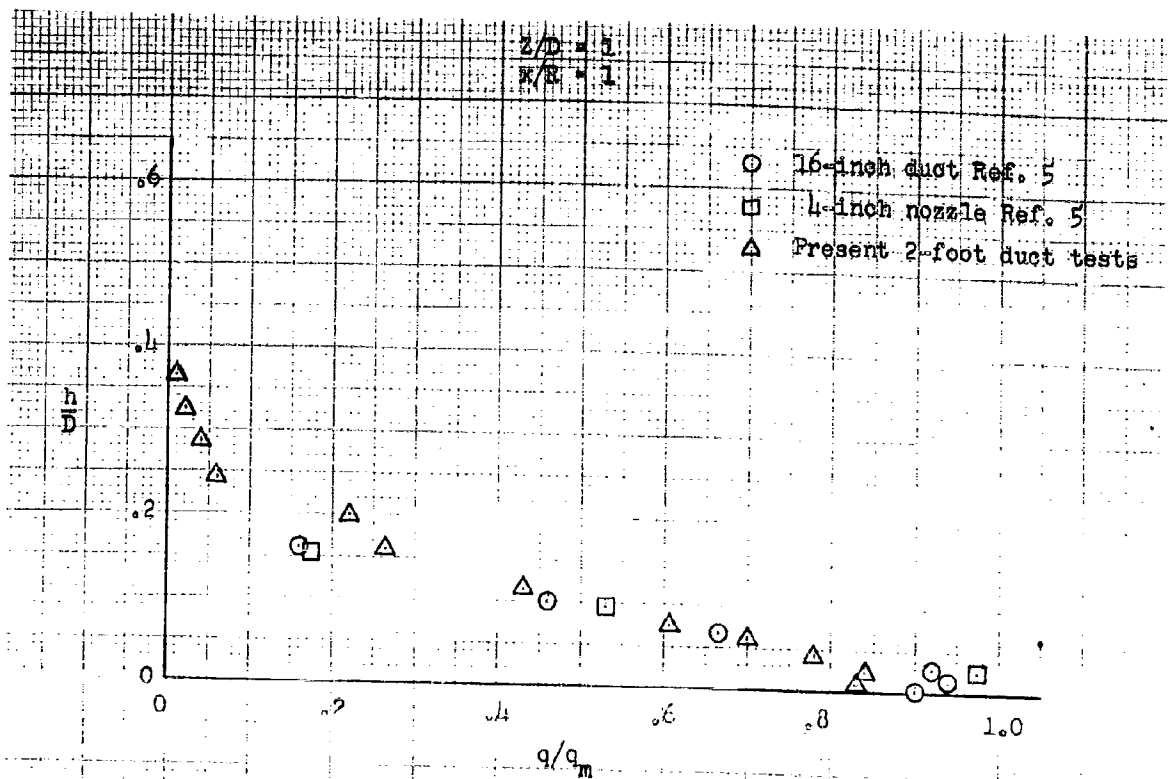


FIGURE 28 COMPARISON OF DYNAMIC-PRESSURE PROFILES AFTER IMPINGEMENT

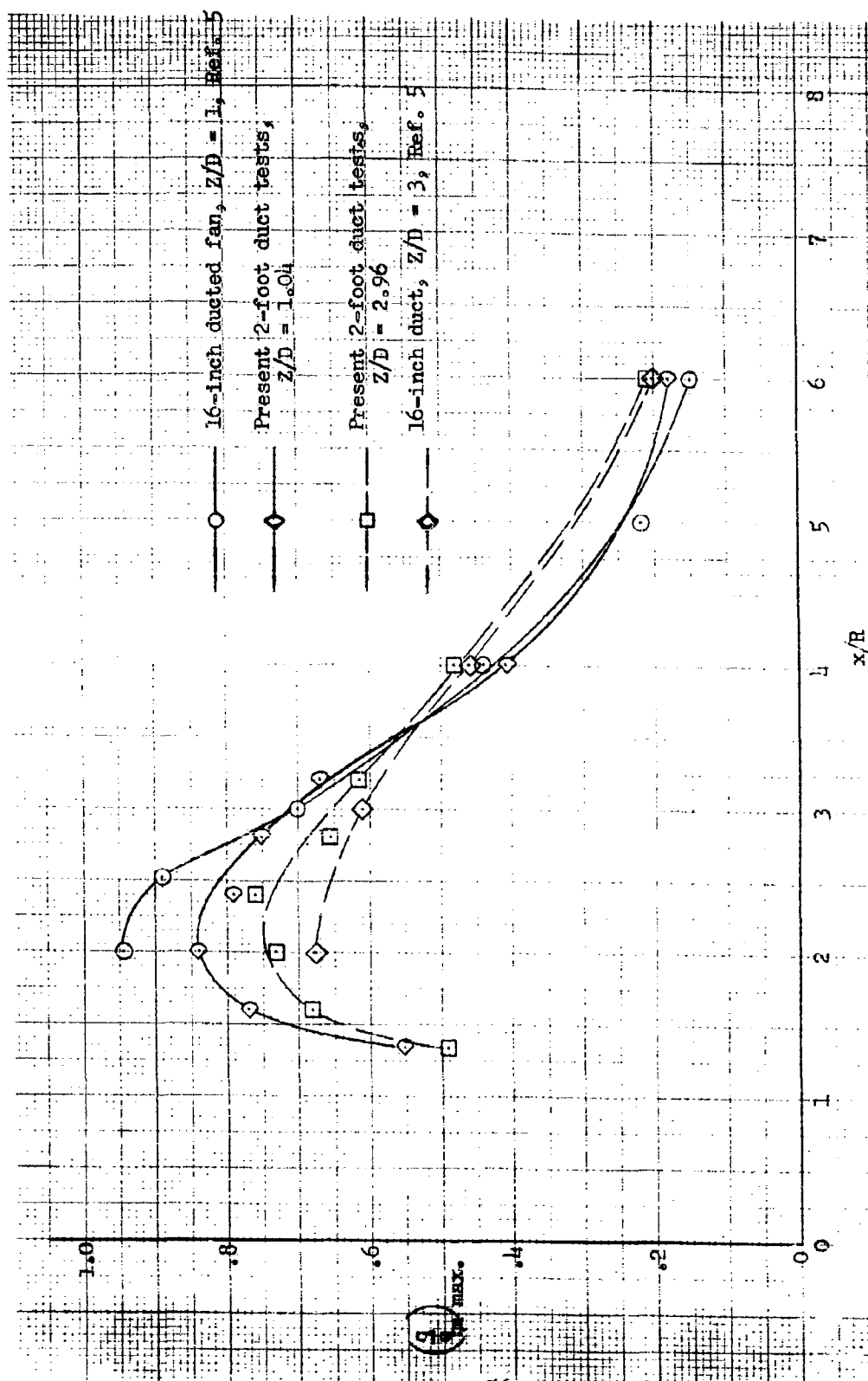


FIGURE 29 VARIATION OF MAX. DYNAMIC-PRESSURE RATIO WITH RADIAL LOCATION

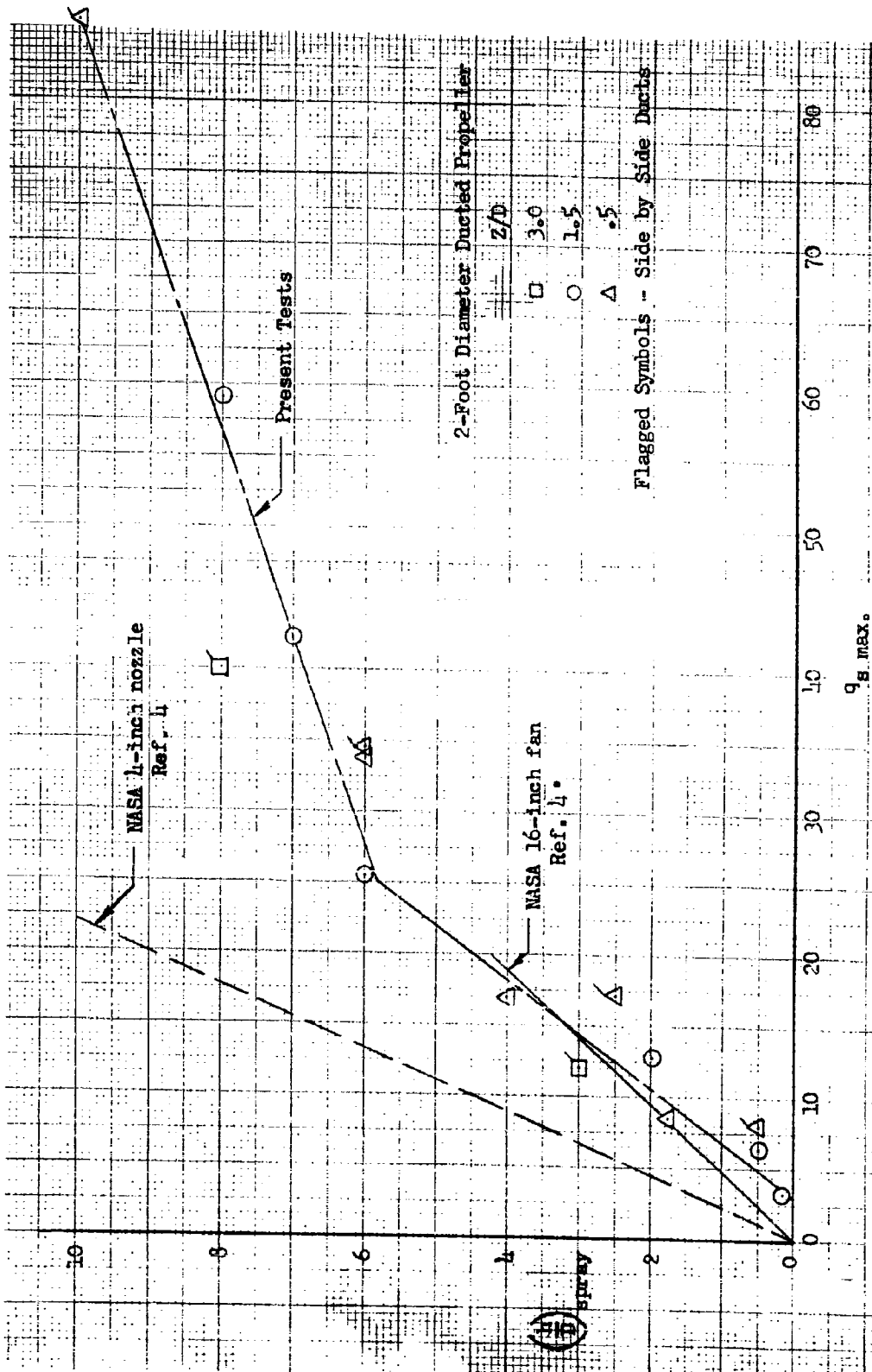


FIGURE 30 OBSERVED SPRAY HEIGHT

7. REFERENCES

1. Morse, A.

"VTOL Downwash Impingement Study, Velocity Survey", TREC Technical Report 60-58.

2. Morse, A.

"VTOL Downwash Impingement Study, Surface Erosion Tests", TREC Technical Report 60-67.

3. Morse, A.

"VTOL Downwash Impingement Study, Duct Adapter Test Program", TREC Technical Report 61-34.

4. Hess, P. J.

"Downwash from Lifting Devices", General Electric, Flight Propulsion Laboratory Department. Propulsion Vol. I, No. 21.

5. Kuhn, Richard E.

"An Investigation to Determine Conditions Under Which Downwash From VTOL Aircraft Will Start Surface Erosion From Various Types of Terrain", NASA TND-56.

APPENDIX

CALCULATIONS LEADING TO A SOLUTION OF THE
FIELD MAXIMUM DYNAMIC PRESSURE IN GROUND EFFECT

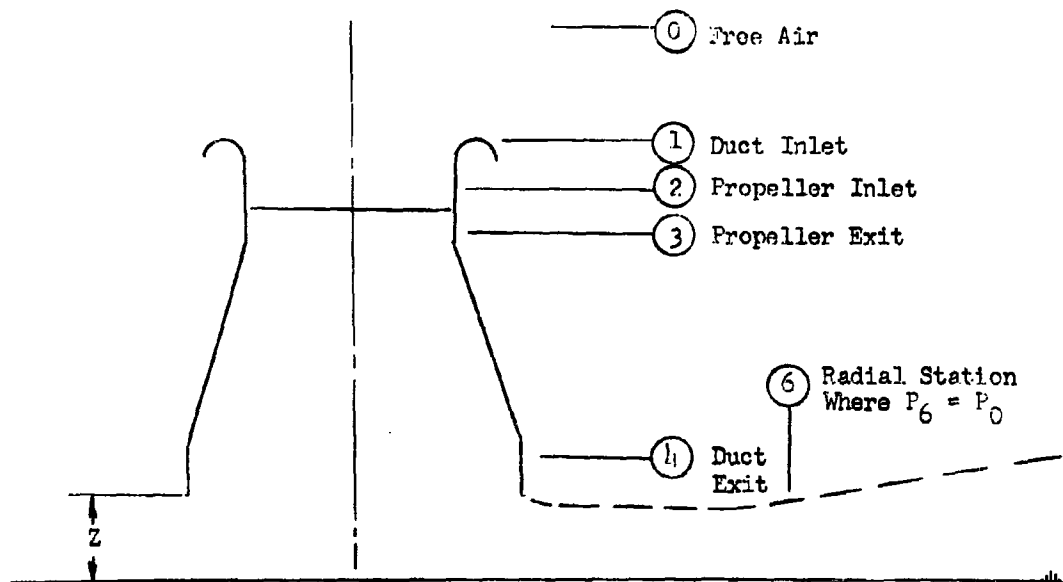
LIST OF SYMBOLS

A_b	= base plate area	square feet
A_4	= duct exit flow area	square feet
c	= periphery of the jet (circumference)	feet
D	= duct exit diameter	feet
F_H	= horizontal force resulting from the surface mass flux	pounds
m	= air mass rate of flow	slugs per second
P	= pressure	pounds per square foot
P'	= power	foot pounds per second
q	= dynamic pressure	pounds per square foot
T_N	= net thrust	pounds
T_{P_6}	= propeller gross thrust	pounds
V	= velocity	feet per second
w	= disk loading	pounds per square foot
z	= duct exit height above the surface	feet
ϵ	= loss coefficient	none
ζ	= A_4/zc	none
η	= efficiency factor	none
ρ	= air mass density	slugs per cubic foot
ϕ	= v_6/v_4	none
ψ	= $q_6/w/2$	none

Subscripts

b = base
d = diffuser
e = effective
G = gross
i = inlet
N = net
P = propeller
T = total

0 to 5 = control stations in the flow field (see sketch below)



If the assumption is made that a uniform pressure exists beneath the dust exit, which is sustained by the radial acceleration of the mass flow, a solution of the mass flow and velocity can be obtained.

P_{T4} is calculated from the horizontal acceleration of the ground flow.

$$\begin{aligned} F_H &= m \Delta V_H = m V_6 \\ F_H &= (P_4 - P_0) Zc \\ P_4 &= \frac{m V_6}{Zc} + P_0 \end{aligned} \quad \text{Equa. (1)}$$

and

$$\begin{aligned} P_{T4} &= P_4 + q_4 \\ \therefore P_{T4} &= \frac{m V_6}{Zc} + P_0 + \frac{\rho V_4^2}{2} \end{aligned} \quad \text{Equa. (2)}$$

A free jet loss is defined as:

$$\epsilon = \frac{P_{T4} - P_{T6}}{q_6}$$

$$\therefore P_{T4} = q_6 \epsilon + P_{T6}$$

$$P_{T6} = P_6 + q_6 \quad \text{but } P_6 = P_0$$

$$P_{T4} = \epsilon q_6 + P_0 + q_6 = q_6(1 + \epsilon) + P_0 \quad \text{Equa. (3)}$$

Equating equations (2) and (3):

$$\frac{m V_6}{Zc} + P_0 + \frac{\rho V_4^2}{2} = P_0 + \frac{\rho V_6^2}{2} (1 + \epsilon)$$

Substituting $m = \rho A_4 V_4$ and multiplying by $\frac{2}{\rho V_4^2 (1 + \epsilon)}$

$$\left(\frac{V_6}{V_4}\right)^2 - \frac{2 A_4 V_6}{Zc(1 + \epsilon) V_4} - \frac{1}{(1 + \epsilon)} = 0$$

$$\frac{V_6}{V_L} = \frac{A_L}{Zc(1+\epsilon)} \left\{ \frac{1}{(1+\epsilon)} + \left[\frac{A_L}{Zc(1+\epsilon)} \right]^2 \right\}^{\frac{1}{2}}$$

$$\frac{V_6}{V_L} = \frac{A_L}{Zc(1+\epsilon)} \left\{ 1 + \left[1 + \left(\frac{Zc}{A_L} \right)^2 (1+\epsilon) \right]^{\frac{1}{2}} \right\} \quad \text{Equa. (4)}$$

Because $(Zc/A_L)^2 (1+\epsilon)$ is positive and V_6/V_L cannot be negative, the positive sign was used.

Now the total thrust can be calculated.

$$T_N = mV_L + A_L(P_L - P_O) + A_b(P_L - P_O)$$

$$T_N = mV_L + (P_L - P_O)(A_L + A_b)$$

from equation (1)

$$P_L - P_O = \frac{mV_6}{Zc}$$

$$T_N = mV_L + \frac{mV_6}{Zc} (A_L + A_b)$$

$$T_N = mV_L \left[1 + \frac{(A_L + A_b)}{Zc} V_6/V_L \right] \quad \text{Equa. (5)}$$

$$V_L = \left\{ \frac{T_N}{A_L \left[1 + \frac{(A_L + A_b)}{Zc} V_6/V_L \right]} \right\}^{\frac{1}{2}} \quad \text{Equa. (6)}$$

To calculate the power, the inlet, diffuser, and propeller losses are required.

Define

Inlet Loss

$$\epsilon_1 = \frac{P_{T0} - P_{T2}}{q_2} = \frac{P_{O0} - P_{T2}}{q_2}$$

Diffuser Loss

$$\epsilon_d = \frac{P_{T3} - P_{T4}}{q_3} = \frac{P_{T3} - P_{T4}}{q_2}$$

Propeller Efficiency $\eta_p = \eta_p$

Now

$$P_{T4} = q_6(1 + \epsilon) + P_0 \quad \text{from Equa. (3)}$$

$$P_{T3} = q_2 \epsilon_d + q_6(1 + \epsilon) + P_0$$

$$P_{T2} = q_2 \epsilon_1 + P_0$$

$$P_{PG} = A_2(P_{T3} - P_{T2}) = A_2(P_{T3} - P_{T2}) \quad q_3 = q_2$$

$$P_{PG} = A_2[q_2 \epsilon_d + q_6(1 + \epsilon) + P_0 + q_2 \epsilon_1 - P_0]$$

$$P_{PG} = q_2 A_2 (\epsilon_d + \epsilon_1) + q_6 A_2 (1 + \epsilon) \quad \text{Equa. (7)}$$

and

$$P' = \frac{P_{PG} V_2}{\eta_p}$$

$$\therefore \eta_p P' = q_2 A_2 V_2 (\epsilon_d + \epsilon_1) + q_6 (A_2 V_2) (1 + \epsilon)$$

$$\frac{2P\eta_p}{mV_6^2} = (1 + \epsilon) + (V_2/V_6)^2 (\epsilon_d + \epsilon_1)$$

$$2P\eta_p = mV_6^2 \left[(1 + \epsilon) (V_6/V_4)^2 + (A_4/A_2)^2 (\epsilon_d + \epsilon_1) \right] \quad \text{Equa. (8)}$$

Combining equations (5), (6) and (8):

$$\frac{2P\eta_p (A_4)^{1/2}}{T_N^{3/2}} = \frac{(V_6/V_4)^{1/2} \left[(1 + \epsilon) + (A_4/A_2)^2 (\epsilon_d + \epsilon_1) \right]}{\left[\frac{1}{V_6/V_4} + \frac{A_4 + A_2}{2c} \right]^{3/2}} \quad \text{Equa. (9)}$$

From Equation (5)

$$T_N = A_L v_L^2 \left[1 + \frac{(A_L + A_b)}{2c} v_6/v_L \right]$$

$$\text{Let } A_T = A_L + A_b$$

$$\frac{T_N}{A_T \int \frac{v_6^2}{2}} = \frac{2 \left[1 + \frac{(A_L + A_b)}{2c} v_6/v_L \right]}{(1 + A_b/A_L) (v_6/v_L)^2}$$

$$\text{Let } T_N/A_T = w$$

$$\frac{w}{2q_6} = \frac{\left[\frac{1}{v_6/v_L} + \frac{(A_L + A_b)}{2c} \right]}{(1 + A_b/A_L) (v_6/v_L)}$$

or

$$\frac{q_6}{w/2} = \frac{(1 + A_b/A_L) v_6/v_L}{\left[\frac{1}{v_6/v_L} + \frac{(A_L + A_b)}{2c} \right]} \quad \text{Equa. (10)}$$

Equations (10) and (4) define the variation of the field maximum dynamic pressure with the physical parameters and the disk loading. If these equations are expressed in terms of diameter for a circular jet, the following relations are obtained.

Equation (4) becomes

$$v_6/v_L = \frac{1}{LZ/D(1+e)} \left\{ 1 + \left[1 + (1+e)(LZ/D)^2 \right]^{\frac{1}{2}} \right\} \quad \text{Equa. (11)}$$

and Equation (10) becomes

$$\frac{q_6}{w/2} = \frac{v_6/v_4 (1 + A_b/A_4)}{\left[\frac{1}{v_6/v_4} + \frac{(A_4 + A_b)}{\pi DZ} \right]}$$

and if $A_b = 0$

$$\frac{q_6}{w/2} = \frac{v_6/v_4}{\left[\frac{1}{v_6/v_4} + \frac{1}{4Z/D} \right]} \quad \text{Equa. (12)}$$

Choosing values of Z/D and solving equations (11) and (12) for $q_6/w/2$ the curves shown in Figure 1 are obtained. For the calculated curve to predict the test results, the free jet loss would have to vary from .1 at $Z/D = .1$ to approximately .35 at $Z/D = 3$.

The value of $2P\eta_P(\sqrt{A_4})^{3/2}/T_N^{3/2}$ (Figure 2) was obtained by substitution in equations (4) and (9) with the assumption that e_d , e_i and A_b are zero and that the jet is circular. The power loading parameter has values greater than one for the case of zero losses ($e = 0$), which is unrealistic; however, the general trend of the maximum surface dynamic pressure ratio and the power loading parameter is encouraging. The parameters for the plenum chamber tests were used to solve equations (4) and (10) with the resulting q_6 value of 1.932 compared to test

$\frac{w/2}$
results in the range of 1.4 to 1.8. The analysis was extended to represent an inclined jet and the parameters for the annular nozzle GEM were used to calculate $q_6/w/2$ with the resulting value of 3.78 obtained. This is compared to the test data where $1.9 \leq q_6 \leq 2.8$.

$\frac{w/2}$
These values were calculated assuming no losses and therefore should be greater than test data values.

This analysis, although non-rigorous, has been shown to provide order of magnitude numbers for three geometrically different jets, and a reasonable relationship between $q_6/w/2$ and Z/D for the circular jet.

It would be worthwhile to examine the equations to determine the influence of the parameters on $q_6/w/2$. Equation (10) can be rewritten in the form:

$$\frac{q_6}{w/2} = \frac{(v_6/v_4)^2}{\left[\frac{1}{(1 + A_b/A_4)} + \frac{A_4}{Z_c} v_6/v_4 \right]} \quad \text{Equa. (10a)}$$

where

$$\frac{v_6}{v_4} = \frac{A_4}{Z_c(1 + \epsilon)} \left\{ 1 + \left[1 + \left(\frac{Z_c^2}{A_4} \right) (1 + \epsilon) \right]^{\frac{1}{2}} \right\} \quad \text{Equa. (4)}$$

These two equations were combined and the first derivative of $q_6/w/2$ was obtained to locate the minimum value. Solutions were found at $A_4/Z_c = 0$ or ∞ , $(1 - \epsilon) = 0$, but no solutions between 0 and ∞ were determined.

The solution of Equation 10a has been represented graphically in Figure 3 with the relation between A_4/Z_c and Z/D for a circular nozzle.

The A_4/Z_c value was calculated for several rectangular jets having aspect ratios of 1, 6 and 16. An equivalent diameter was then obtained, the equivalent diameter is defined as the diameter of a circular jet of the same total cross sectional area as the rectangular jet. Figure 4 was then constructed to present the effect of aspect ratio on the $q_6/w/2$ parameter.

The power loading disk loading parameter $2P' \eta_P (\rho A_4)^{\frac{1}{2}} / T_N^{3/2}$ can be related to the field maximum dynamic pressure.

$$\text{Let } A_b = 0, (\epsilon_i + \epsilon_d) = 0, \epsilon = 0, v_6/v_4 = \phi, \frac{A_4}{Zc} = \zeta$$

$$\text{and } q_6/w/2 = \psi$$

from Equation (9)

$$\frac{2F' \eta_P (\rho A_4)^{\frac{1}{2}}}{T_N^{3/2}} = \frac{\phi^{\frac{1}{2}}}{\left(\frac{1}{\phi} + \zeta\right)^{3/2}} = \frac{\phi^2}{(1 + \zeta \phi)^{3/2}}$$

and from Equation (10a)

$$\psi = \frac{\phi^2}{(1 + \zeta \phi)}$$

$$\text{or } \frac{2F' \eta_P (\rho A_4)^{\frac{1}{2}}}{T_N^{3/2}} = \frac{\psi}{(1 + \zeta \phi)} = \frac{q_6}{w/2 \left(1 + \frac{A_4}{Zc} v_6/v_4\right)^{\frac{1}{2}}}$$

Therefore, any reduction in $q_6/w/2$ will reflect in a reduction in power loading, which would be desirable, and a high aspect ratio jet would be desirable when operating in ground effect.

Circular Jet
No Base Plate

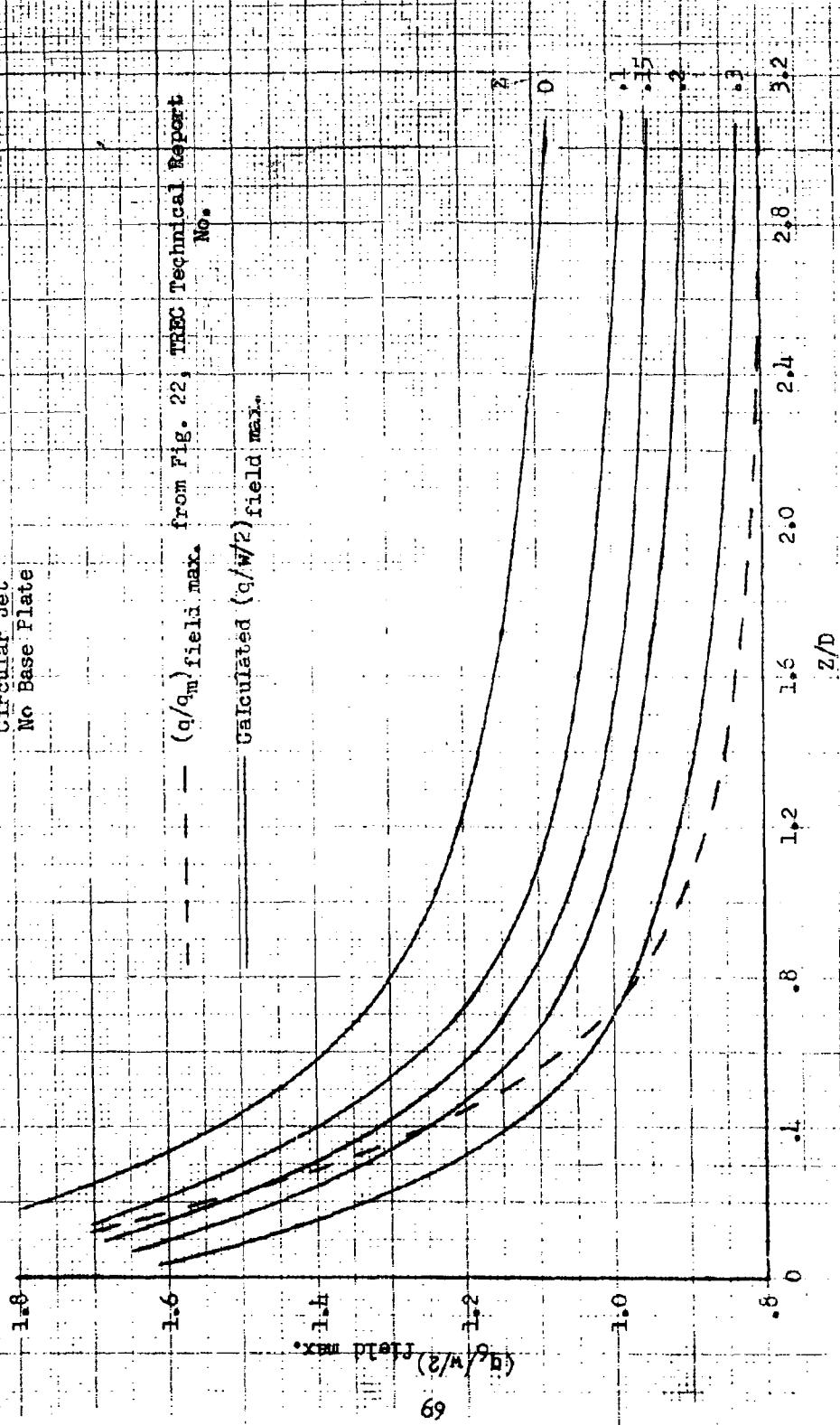


Figure 1 Maximum Surface Dynamic Pressure with Losses

Figure 2 Power Loading - Disk Loading
Parameter Variation with Z/D

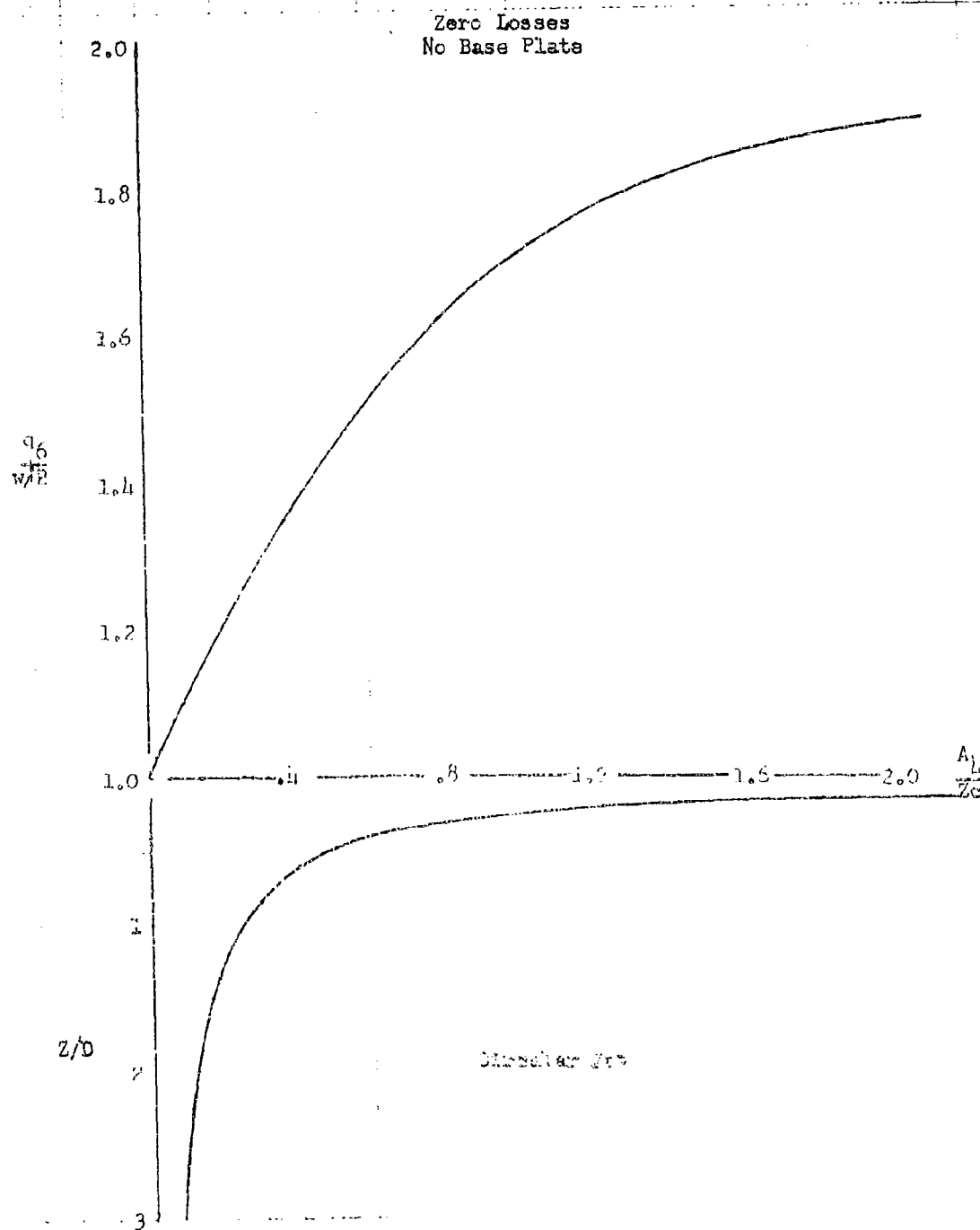


Figure 3 Maximum Surface Dynamic Pressure
as Influenced by Ground Effect

Based on Equal Exit Area
No Losses

Round Jet
Aspect Ratio = 1
6
16

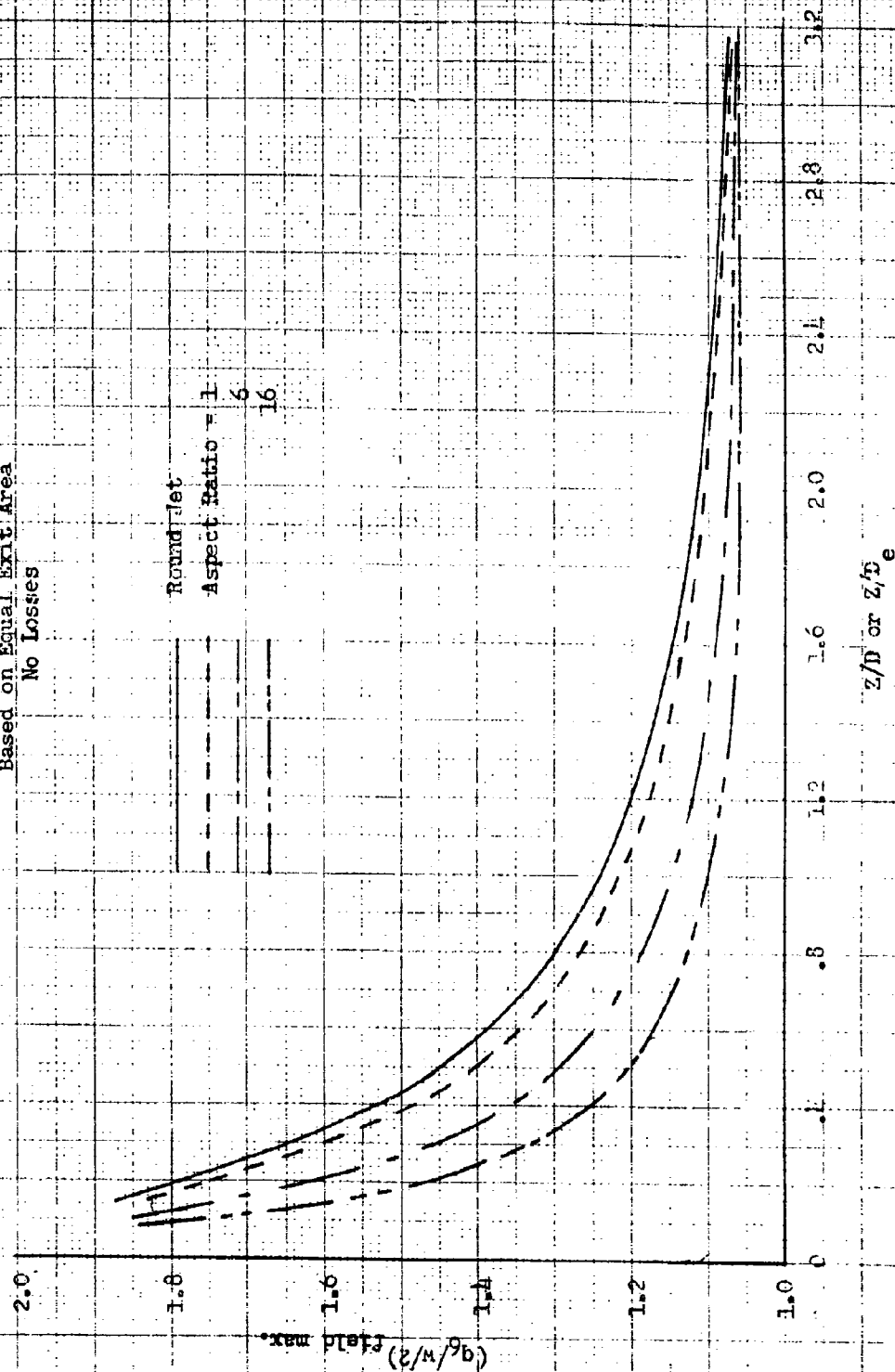


Figure 4 Effect of Aspect Ratio on
Maximum Surface Dynamic Pressure

DISTRIBUTION LIST
for
VTOL DOWNWASH IMPINGEMENT STUDY, SUMMARY REPORT

Chief of Transportation
ATTN: TODRD
Department of the Army
Washington 25, D. C. (2)

Commanding Officer
U. S. Army Transportation Research Command
ATTN: Executive for Programs (1)
ATTN: DCO for Aviation (1)
ATTN: Long Range Technical Forecast Office (1)
ATTN: Aviation Directorate (2)
ATTN: Research Reference Center (4)
ATTN: Military Liaison & Advisory Office (4)
Fort Eustis, Virginia

Commanding Officer
U. S. Army Transportation Research Command Liaison Office
ATTN: MCLATS
Wright-Patterson Air Force Base, Ohio (1)

Chief of Research and Development
ATTN: Air Mobility Division
Department of the Army
Washington 25, D. C. (1)

Commander
Aeronautical System Division
ATTN: WWRMPT-1
Air Force Systems Command
Wright-Patterson Air Force Base, Ohio (1)

Chief of Naval Research
Code 461, Maj. L. C. Robertson
Washington 25, D. C. (1)

Chief, Bureau of Naval Weapons
ATTN: RAAD-322
Department of the Navy
Washington 25, D. C. (1)

Chief of Engineers
ATTN: Mr. W. V. Kreipke
Department of the Army
Washington 25, D. C. (1)

Director
 U. S. Army Engineer Waterways Experiment Station
 ATTN: Chief, Flexible Pavements Branch (1)
 Corps of Engineers
 Vicksburg, Mississippi

Commander
 Armed Services Technical Information Agency
 ATTN: TIPCR (10)
 Arlington Hall Station
 Arlington 12, Virginia

Civil Aeronautics Board
 Safety Analysis Division
 Bureau of Safety
 Washington 25, D. C. (1)

Librarian
 Langley Research Center
 National Aeronautics and Space Administration
 Langley Field, Virginia (2)

John J. Glennon, Librarian
 Institute of the Aerospace Sciences
 2 E. 64th Street
 New York 21, New York (1)

Aero-Space Division
 Boeing Airplane Company
 ATTN: Aircraft Development Section (1)
 P. O. Box 3707
 Seattle 24, Washington

Bell Aerosystems Company
 Division of Bell Aerospace Corporation
 ATTN: Library (1)
 Buffalo 5, New York

Bell Helicopter Company
 Division of Bell Aerospace Corporation
 ATTN: Library (1)
 P. O. Box 482
 Fort Worth 1, Texas

Chance Vought Aircraft, Incorporated
 Vought Aeronautics Division
 Box 5907
 Dallas 22, Texas (1)

Cornell Aeronautical Laboratory, Inc.

4455 Genesee Street
Buffalo 21, New York

(2)

Convair Division
General Dynamics Corporation
ATTN: Library
San Diego, California

(1)

Aeronautics Division
Ford Motor Company
ATTN: Library
5656 E. Slauson Avenue
Los Angeles, California

(1)

Kellett Aircraft Corporation
ATTN: Library
P. O. Box 35
Willow Grove, Pennsylvania

(1)

Lockheed Aircraft Corporation
ATTN: Library
Marietta, Georgia

(1)

Communication Services Group
North American Aviation, Inc.
ATTN: RFD 8913
4300 East Fifth Avenue
Columbus 16, Ohio

(1)

Sikorsky Aircraft
Division of United Aircraft Corporation
ATTN: Library
Stratford, Connecticut

(1)

AD

Accession No.
 Miller Aircraft Corp., Palo Alto, California
 VTOL Downwash Impingement Study, Summary Report - A. Morse
 Miller Report No. 61-3, August 1961, 75 pp. (Contract DA 44-177-TC-655)
 UNCLASSIFIED Task 9830-01-017-29

A test program was conducted and reports were published to provide early availability of the data. This program was designed to provide fundamental background information and to aid in the evaluation of operational problems associated with the albatross impingement. This report is a summary of the results of the entire program. Configurations used in this program consisted of: open propellers, ducted propellers, side by side jets, and ground effect machines of the plenum and nozzle types. Disk loadings of 2 to 350 pounds per square foot and 2/0 ratios of .25 to .3 were investigated. Data was obtained to determine: the over-all jet pattern, flow velocities, erosion rates for various soils, and the surface deflection and spray height caused by operation over water.

The maximum field dynamic pressure resulting from the impingement was determined to be a function of 2/0 and disk loading and was found to be the parameter governing the erosion onset and the maximum surface deflection for operation over water.

Dry loose material such as sand, dust, dry grass, etc., erode when the surface dynamic pressure is three pounds per square foot, or less. Water spray starts to form in the same range of surface dynamic pressures. May natural surfaces will withstand surface dynamic pressures above 150 pounds per square foot with very minor damage. The loose surface material produces clouds of airborne particles that reduce visibility and are the principal cause of most of the operational problems.

UNCLASSIFIED

1. Free Jet Impingement
2. E-57C

3. Slipstream, Propeller
4. Surface Erosion
5. Operational Problems, General

- I. A. Morse
- II. Contract DA 44-177-TC-655

AD

Accession No.
 Miller Aircraft Corp., Palo Alto, California
 VTOL Downwash Impingement Study, Summary Report - A. Morse
 Miller Report No. 61-3, August 1961, 75 pp. (Contract DA 44-177-TC-655)
 UNCLASSIFIED Task 9830-01-017-29

A test program was conducted and reports were published to provide early availability of the data. This program was designed to provide fundamental background information and to aid in the evaluation of operational problems associated with the albatross impingement. This report is a summary of the results of the entire program. Configurations used in this program consisted of: open propellers, ducted propellers, side by side jets, and ground effect machines of the plenum and nozzle types. Disk loadings of 2 to 350 pounds per square foot and 2/0 ratios of .25 to .3 were investigated. Data was obtained to determine: the over-all jet pattern, flow velocities, erosion rates for various soils, and the surface deflection and spray height caused by operation over water.

The maximum field dynamic pressure resulting from the impingement was determined to be a function of 2/0 and disk loading and was found to be the parameter governing the erosion onset and the maximum surface deflection for operation over water.

Dry loose material such as sand, dust, dry grass, etc., erode when the surface dynamic pressure is three pounds per square foot, or less. Water spray starts to form in the same range of surface dynamic pressures. May natural surfaces will withstand surface dynamic pressures above 150 pounds per square foot with very minor damage. The loose surface material produces clouds of airborne particles that reduce visibility and are the principal cause of most of the operational problems.

AD

Accession No.
 Miller Aircraft Corp., Palo Alto, California
 VTOL Downwash Impingement Study, Summary Report - A. Morse
 Miller Report No. 61-3, August 1961, 75 pp. (Contract DA 44-177-TC-655)
 UNCLASSIFIED Task 9830-01-017-29

A test program was conducted and reports were published to provide early availability of the data. This program was designed to provide fundamental background information and to aid in the evaluation of operational problems associated with the albatross impingement. This report is a summary of the results of the entire program. Configurations used in this program consisted of: open propellers, ducted propellers, side by side jets, and ground effect machines of the plenum and nozzle types. Disk loadings of 2 to 350 pounds per square foot and 2/0 ratios of .25 to .3 were investigated. Data was obtained to determine: the over-all jet pattern, flow velocities, erosion rates for various soils, and the surface deflection and spray height caused by operation over water.

The maximum field dynamic pressure resulting from the impingement was determined to be a function of 2/0 and disk loading and was found to be the parameter governing the erosion onset and the maximum surface deflection for operation over water.

Dry loose material such as sand, dust, dry grass, etc., erode when the surface dynamic pressure is three pounds per square foot, or less. Water spray starts to form in the same range of surface dynamic pressures. May natural surfaces will withstand surface dynamic pressures above 150 pounds per square foot with very minor damage. The loose surface material produces clouds of airborne particles that reduce visibility and are the principal cause of most of the operational problems.

AD

Accession No.
 Miller Aircraft Corp., Palo Alto, California
 VTOL Downwash Impingement Study, Summary Report - A. Morse
 Miller Report No. 61-3, August 1961, 75 pp. (Contract DA 44-177-TC-655)
 UNCLASSIFIED Task 9830-01-017-29

A test program was conducted and reports were published to provide early availability of the data. This program was designed to provide fundamental background information and to aid in the evaluation of operational problems associated with the albatross impingement. This report is a summary of the results of the entire program. Configurations used in this program consisted of: open propellers, ducted propellers, side by side jets, and ground effect machines of the plenum and nozzle types. Disk loadings of 2 to 350 pounds per square foot and 2/0 ratios of .25 to .3 were investigated. Data was obtained to determine: the over-all jet pattern, flow velocities, erosion rates for various soils, and the surface deflection and spray height caused by operation over water.

The maximum field dynamic pressure resulting from the impingement was determined to be a function of 2/0 and disk loading and was found to be the parameter governing the erosion onset and the maximum surface deflection for operation over water.

Dry loose material such as sand, dust, dry grass, etc., erode when the surface dynamic pressure is three pounds per square foot, or less. Water spray starts to form in the same range of surface dynamic pressures. May natural surfaces will withstand surface dynamic pressures above 150 pounds per square foot with very minor damage. The loose surface material produces clouds of airborne particles that reduce visibility and are the principal cause of most of the operational problems.